Carbon monoxide gas sensing properties of a Metal-Oxide-Semiconductor capacitor sensor

Jeffrey Christopher Hunter
B.S., Electrical Engineering. University of New Mexico (1995)

A thesis presented to the faculty of the
OGI School of Science & Engineering
at Oregon Health & Science University
in partial fulfillment of the
requirements for the degree
Master of Science
in
Electrical Engineering

October 2003

Copyright 2003, Jeffrey C. Hunter

The thesis "Carbon Monoxide Gas Sensing Properties of a Metal-Oxide-Semiconductor Capacitor Sensor" by Jeffrey Christopher Hunter has been examined and approved by the following Examination Committee:

Dr. Jack McCarthy,
Assistant Professor
Thesis Research Advisor

Dr. Raj Solanki
Professor

Dr. John L. Freeouf
Professor

Acknowledgements

I would like to acknowledge Professor Jack McCarthy for his tremendous support and mentoring in this investigation and experimentation direction and his contributions to the sensor thin film characterization and material microanalysis. Also, many thanks to Jim Pankow from the OGI Environmental Systems Engineering group for providing use of his tremendous laboratory facility and Lorne Isabelle for working with me to develop and construct a gas flow test system capable of precisely controlling carbon monoxide concentrations during exposure and a testing methodology. Also, thanks to Professor Raj Solanki for allowing me to utilize his top notch semiconductor characterization lab and equipment and Bill Meyer for training me on use of the electrical test prober and measurement equipment.

Contents

List of Tables

List of Figures

Abstract

Carbon Monoxide Gas Sensing Properties of a Metal-Oxide-Semiconductor Capacitor Sensor

Jeffrey C. Hunter, B.S.

M.S., OGI School of Science & Engineering

at Oregon Health & Science University

September 2003

Thesis Advisor: Dr. Jack McCarthy

New MOS (metal-oxide-semiconductor) field-effect gas sensors capable of detecting carbon monoxide at low concentrations and operating temperatures are fabricated and tested. A catalytic multi-layer gate system is presented composed of a 60 nm iron oxide nanoparticle film deposited by thermal evaporation and an additional 60 nm platinum surface layer gate electrode film deposited using direct pattern focused ion beam (FIB) deposition. The sensor integrates the catalytic properties of a highly diffusive platinum thin film and the gas absorptive properties of iron oxide, both mechanisms previously shown to independently produce work function changes in an MOS capacitor in the presence of carbon monoxide. Additional sensor configurations are also evaluated utilizing only platinum as the surface sensing mechanism with thicknesses of 30 nm and 60 nm. The morphology and characteristics of the gate films are studied using scanning electron and transmission electron microscopy and x-ray micro-analysis. High frequency capacitance-voltage measurements are made at various carbon monoxide concentration levels and operating temperatures of 23 °C and 200 °C. The 30 nm and 60 nm thick Pt only sensors are shown to detect at room temperature carbon monoxide in dry air at concentration levels of less than 1000 ppm with measurable voltage shifts of 200 mV and 150 mV at 25 ppm CO respectively. The Pt/iron oxide multi-layer film sensor revealed a measurable change in capacitance of 6.5 pF with an absence of a flat-band voltage shift at 1000 ppm.

Introduction

Semiconductor field-effect gas sensors of various material composition and configuration have been successfully designed and manufactured to detect trace amounts of numerous types of gas for the last thirty years. At the heart of a field-effect gas sensor is the metal-oxide-semiconductor (MOS) capacitor stack and its change in the electrical response when exposed to an analyte gas due to the chemical reaction between the metallic gate and gas.

Perhaps the most well known and best understood solid state sensor was the palladium hydrogen MOS sensor developed by Lundstrom [1] with a sensing mechanism well explained by the Langmuirian model [2]. Hydrogen atoms formed by dissociation on the Pd surface rapidly diffuse through a thin metal gate and become trapped at the Pd/SiO_2 interface, forming a dipole charge layer, thus creating a flat band voltage shift in the capacitor due to the trapped charges. Figure 1.1 below is a diagram created by Lundstrom et al. to show the two primary sensing chemistries used in solid state gas sensors [3]. It has also been shown that the threshold voltage may shift negatively or positively depending on the reaction behavior between the catalytic metal and gas being sensed and the associated dipole charge created in the sensing film. The amplitude of the flat band voltage shift will increase as a function of gas concentration and operating temperature used to stimulate the surface reaction. Lundstrom demonstrated voltage shifts on the order of 500mV at pressures around 1 Torr and 200 °C [3].

Gas sensors made today take full advantage of the maturity and availability of semiconductor device fabrication equipment and complementary MOS (CMOS) processing methods. Millions of sensors can be arrayed on a microchip and integrated with signal processing circuits and larger electronic systems. Numerous MOS based sensors exist in the

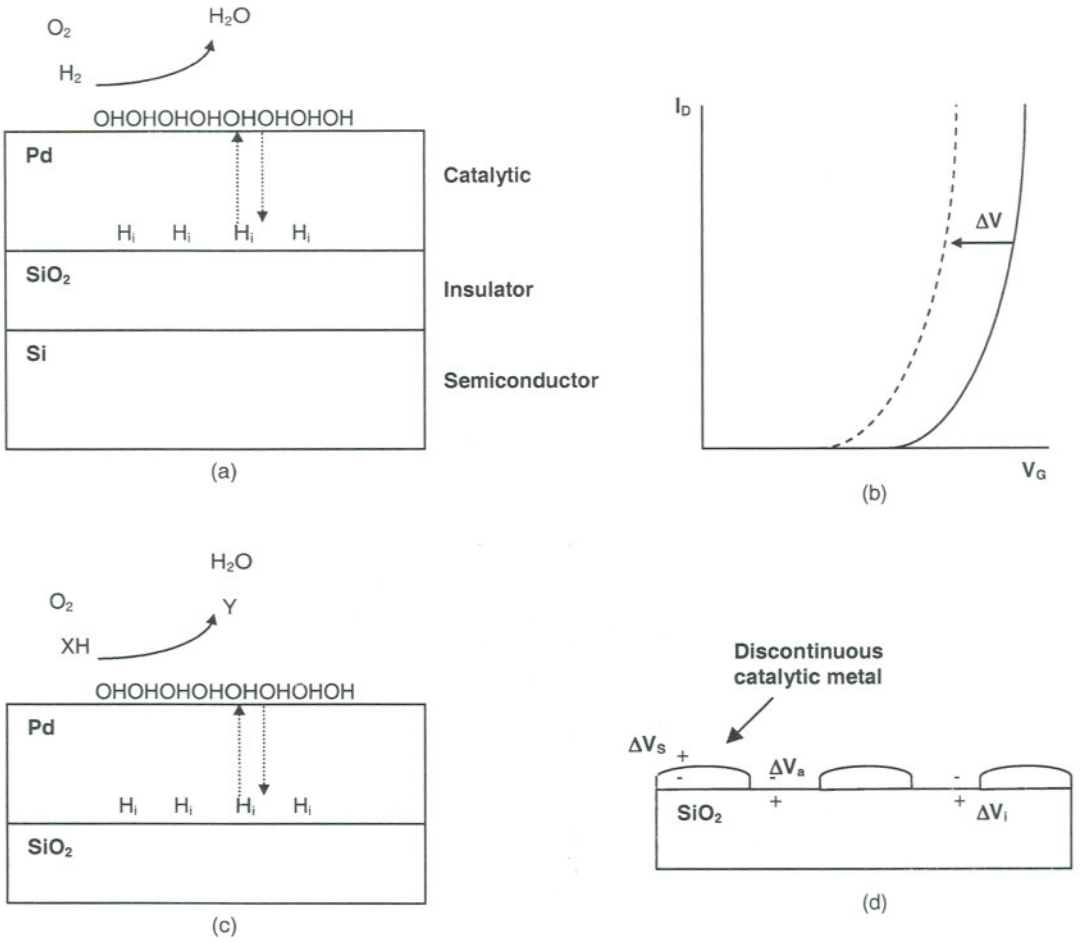

Figure 1.1: Principles of gas sensitive field-effect sensors. (a) Hydrogen sensitive thick Pd gate. (b) Affect of threshold voltage shift in MIS capacitor due to chemically induced polarization phenomena. (c) Thick gate detects all molecules which deliver hydrogen atoms to the catalytic metal film. (d) Thin discontinuous or porous metal gate detects several types of chemically induced polarization phenomena at the surface (s) and interface (i) of the catalytic metal and on the insulator (a) [Ref. 3]

marketplace to detect common analytes such as hydrogen, nitrogen, and carbon based gases such as H_2, NH_4, NO_2, CO, and CO_2.

Not all catalytic metals are appropriate for sensing particular gases. Pd and Pt have been shown to be very effective in sensing hydrogen based gases and additionally, Pt has shown some sensitivity to carbon monoxide and combustible gases in general [3]. Gold has been shown to be very useful in detecting nitrous oxides, even at room temperature. Filippini et al. demonstrated a thick film Au-gate solid state sensor capable of detecting flat

band voltage shifts of 2.72 mV/ppm at 140 ppm concentration of NO_2 in dry air [4]. Metal oxides such as tin oxide (SnO_2), nickel oxide (NiO), and iron oxide (primarily in a stable hematite formation of Fe_2O_3), and mixed oxide compounds such as titanium-tungsten oxide (Ti-W-O) have demonstrated effective sensing of combustible gases including CO [5,6]. Comini et al. demonstrated a sensor with a Mo-W-O metal oxide gate composition had a detectable response of 40 pA for CO concentrations less than 60 ppm with a recovery time of 2 minutes [6].

Solid state gas sensors are typically operated at high temperatures in the range of 150 to 400 °C to decrease absorption time of the sensed gas and expedite reversibility of charged particles trapped in the metal-oxide stack and interface, attained typically through a chemisorption process. Typical test chip designs include an interdigitated heater located on the backside surface which is then connected to a heater control element. In one design example, Comini et al. demonstrated response and recovery times of 30 to 90 seconds at operating temperatures greater than 250 °C and greater than 200 seconds at lower temperatures for a MOS sensor consisting of a TiO_2 and Fe_2O_3 gate metal stack [5]. Filippini et al. reported decreasing response and recovery times for a tin oxide MOS sensor detecting NO_2 at temperatures ranging from 100 to 200 °C in 100 minute exposure intervals [7]. There have been several published examples of sensors operating effectively at room temperature. Detectable responses in the range of 50 to 100mV were demonstrated by Kasama et al. for a Pt/SnO_x sensor exposed to 100 ppm concentration of CO at room temperature [8].

Thin film morphology has been shown to strongly affect gas sensitivity and selectivity. Morphology is analyzed in terms of dislocations or porosity of the film, surface roughness, and grain size. Porosity has been shown to be of particular importance as it aids in the diffusion of larger analyte gas molecules to the dielectric substrate allowing a dipole layer to form, increasing response sensitivity. It is hypothesized by Filippini et al. that in the diffusion process during the exposure reaction, gas permeates along the metal grain boundaries to the dielectric surface [7]. Thus smaller grains provide more diffusion paths in the film. Film morphology is affected by the deposition method, substrate temperature during operation, and film thickness. In Lundstrom's evaluation of platinum hydrogen sensor response for a range of film thicknesses, it was shown that a thin discontinuous film, generally less than 70 nm, exhibited an increased response and sensitivity as compared to

thicker films [3]. A thin gate was defined as a metal gate film that did not completely cover the oxide surface. Discontinuous catalytic gates were shown to detect several types of chemically induced polarization phenomena at the surface and interface of the catalytic metal and on the insulator. In the classic palladium gate hydrogen sensor, a thick gate film was used, only letting hydrogen atoms diffuse through the film to the oxide surface. Only diffused hydrogen ions formed dipole charges at the metal-insulator interface [1]. In fact it was shown by Lofdahl et al. that a Pd film showed no H_2 detection sensitivity at a thickness less than 10 nm and performed best exhibiting a 450 mV shift at a thickness greater than 50 nm [9]. Platinum has traditionally shown poorer response to H_2 than palladium, however measurable responses are still observed. Lofdahl et al. also revealed that at Pt film thicknesses ranging from 4 nm to 70 nm optimum response was found between 10 and 30 nm [9]. Chang et al. evaluated the sensitivity of ZnO:Al films at different thicknesses in detecting CO and found that a 65 nm film was 40% more sensitive to a 1000 ppm concentration than a 280 nm film, a film nearly four times as thick [10]. Further, Lofdahl et al. compared film thickness versus response sensitivity for Pd, Pt, and Ir gate metal films for H_2, NH_3, C_2H_4, CH_3CHO, and C_2H_5OH. In the case of Pt, an optimum response was found at less than 15 nm for all gases and had the sharpest response difference for ammonia of approximately 900 mV [11]. Other recent research has introduced the concept of adding thin oxide films as surface modifiers to enhance the selectivity of the gas sensor. Abom et al. found that less than 10 nm SiO_2 and SnO_2 films deposited on Pt changed the catalytic reaction towards greater NH3 selectivity [12].

Carbon monoxide detection is of utmost importance as it is the gas produced due to incomplete combustion processes from sources like car engines and exhaust systems and is toxic at even low concentrations. In the United States, a concentration of 50 ppm CO in normal atmosphere is the maximum tolerable concentration limit allowed in the work place for an 8 hour exposure [13]. In this investigation, new field-effect MOS capacitor sensors capable of sensing carbon monoxide gas are reviewed, utilizing a unique gate construction consisting of nanometer scale layers of focused ion beam deposited Pt and evaporated iron oxide. Both materials have been shown to be capable of independently detecting CO gas at small concentrations. The dual layer configuration of Pt and iron oxide is expected to utilize both the catalytic properties of Pt and the strong chemical reaction properties of CO with iron oxide [5, 14]. Specifically, iron oxide has favorable reduction reactions in the presence

of carbon monoxide as shown below in Figure 1.2, and has been classified as an n-type semiconductor with a wide energy band gap [15].

$$3Fe_2O_3 + CO \rightarrow 2Fe_3O_4 + CO_2$$
$$Fe_3O_4 + CO \rightarrow 3FeO + CO_2$$
$$FeO + CO \rightarrow Fe + CO_2$$

Figure 1.2: Common reduction reactions of iron oxide and carbon monoxide gas [15]

Further, both metals have showed the capability of detecting CO gas at temperatures well below 400 °C. In general, the sensing films are deposited at very fine thicknesses of less than 100 nm and in methods to achieve film grain sizes of less than 100 angstroms in diameter. As shown through prior research, it is expected that thin films with fine grain sizes will optimize diffusion of the carbon monoxide gas molecules through to the oxide surface and optimize the amount of catalytic metal atomic surface area available to interact with the diffusing gas to form trapped charges. Three specific new gate configurations are evaluated: 1) 60 nm Pt gate contact and 100 nm iron oxide film on 1 μm SiO_2, 2) 30 nm Pt gate metal on 7 nm SiO_2, and 3) 60 nm Pt gate metal on 7 nm SiO_2. The iron oxide is deposited by thermal evaporation at high temperature from stoichiometric hematite (Fe_2O_3) powder and the platinum is deposited using direct pattern focused ion beam metal deposition, not used in previous MOS gas sensor designs. Focused ion beam deposition has been shown to produce robust films with grain sizes of less than 50 angstroms. However, the as deposited film consists not only of the desired metal (Pt) but also the source ions used and by-products of the ion milling process, in this case gallium and carbon, and their effect on the sensing process will need to be assessed.

Principles of Operation

The principle sensing mechanism of an MOS gas sensor is the intrinsic shift in gate capacitor flat band voltage, V_{FB}, defined below in Equation 2.1,

$$2.1 \qquad V_{FB} = \Phi_{ms} - Q_f/C_{ox} - Q_m/C_{ox} - Q_{ot}/C_{ox} - Q_{it}/C_{ox} \text{ and}$$

$$2.2 \qquad C_{ox} = \varepsilon_{ox}/t_{ox}$$

where Φ_{ms} is the work function difference between the metal and doped silicon substrate, Q_f (fixed trapped charge), Q_m (mobile oxide charge), Q_{ot} (oxide trapped charge), and Q_{it} (interface trapped charge) are the quantities of types of trapped charges present in the oxide and at the interfaces, and C_{ox} is the oxide capacitance per unit area [16]. In Equation 2.2, t_{ox} is the oxide thickness and ε_{ox} is the dielectric permittivity (product of the dielectric constant and permittivity of free space). The voltage shift is due to a net change in quantity of trapped charges formed primarily in the metal surface layer and at the oxide interface due to the reaction between the gate metal and adsorbed gas molecules as illustrated in Figure 1.1d. Thus the total voltage shift, ΔV_{total}, can be characterized as:

$$2.3 \qquad \Delta V_{total} = g\Delta V_i + g\Delta V_s + g_a\Delta V_a,$$

where the g_n's are electrostatic coupling coefficients representing the electrostatics of the thin film and the ΔV_n's are the net voltage shifts at the interface, surface, and on the insulator shown in Figure 1.1d and both are dependent on film's intrinsic structure [3]. Further, the flat band voltage will shift positively or negatively depending on whether it is an n-type or p-type semiconductor and the net trapped charge value. In the sensors described in this paper

there are two primary gate film constructions considered: 1) 100x100 μm of 60 nm thick Pt metal on top of 500 μm diameter of 100 nm thick iron oxide, 2) 100x100 μm of 60 or 30 nm thick Pt metal, as shown below in Figure 2.1.

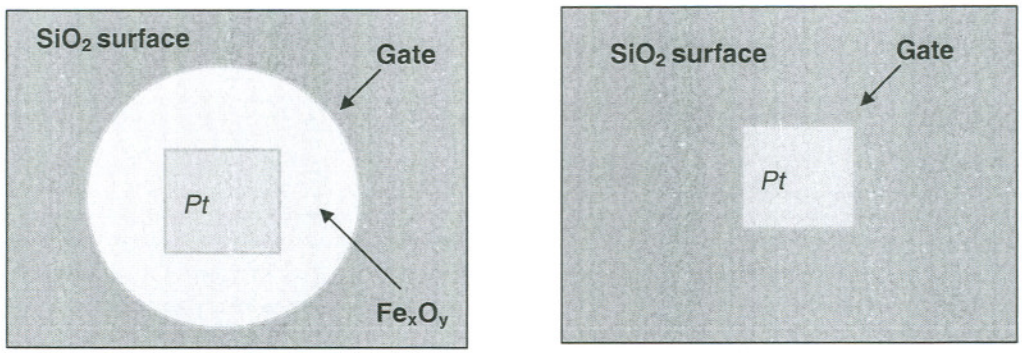

(a) (b)

Figure 2.1: Proposed CO monitoring gas sensor gate configurations

The sensing process is believed to function as follows: 1) in air, oxygen adsorbs on the surface of iron oxide or Pt and reversibly extracts an electron forming adsorbed O^-, O^{2-}, or O_2^-, increasing the film's resistance, 2) when CO is present, the gas reacts irreversibly with the adsorbed forms of oxygen to form CO_2 and released electrons (oxygen behaves as an acceptor) in the film thereby reducing the resistance,

(1) $O_2 + 2e^-$ (extracted from metal oxide) $\rightarrow 2O^-$ (adsorbed oxygen)

(2) $CO + O^- \rightarrow CO_2 + e^-$ (released electron)

Figure 2.2: Chemical reactions causing changes in conductivity of a metal oxide film [17]

3) the film resistance decreases with increasing CO concentration, and finally 4) heating of the substrate increases the overall chemical reaction rate [17]. By changing the concentration

of acceptors in the metal oxide, the conductivity of the space-charge region is modulated. It has been shown that the film thickness should be kept approximately equal to the induced depletion region depth. Catalysts such as platinum are deposited on the surface to speed up the combustion reaction and thus response of the sensor, as noted: $O_2 + 2Pt \rightarrow 2(Pt - O)$. A catalyst is a substance which has an effect of increasing the reaction rate by lowering the activation energy of a chemical reaction without itself undergoing a chemical change [18]. During sensor operation, a bias voltage is applied to the MOS capacitor gate and is swept from negative to positive voltage producing a response in actual capacitance. In the presence of the CO gas, the C-V response is shifted negatively due to the accumulation of acceptor electrons from the gas. This shifted curve is compared against the initial baseline curve calculating a voltage shift, ΔV, representing the amplitude of response sensitivity. Sensor operating temperature is increased to enhance the reaction rate and characterize differences in sensitivity response with the addition of thermal energy. Finally, the analyte gas concentration is varied from concentrations less than 100 ppm in dry air to relatively high concentrations on the order of 1000 ppm. In general, greater sensor response is expected at higher CO concentration and operating temperature.

Sensor Design

The MOS sensor designs reviewed in this investigation include three core components: 1) thin film catalytic Pt gate electrode deposited using focused ion beam metal deposition, 2) thermal silicon dioxide dielectric layer, and 3) a p-type (100) doped substrate. In one design, the use of iron oxide as a diffusion metal layer to trap additional charges was tested due to the metal oxide's well known reaction properties with carbon monoxide. Thinner films and small grains are known to aid gas diffusion to the dielectric layer. In Abom et. al, a the oxide film surface modifier was deposited on top of a thin porous Pt film and gate voltage was applied directly to an aluminum contact attached to the Pt metal thereby minimizing changes to a classic MOS C-V response [12]. In this experiment, the iron oxide film is integrated into the MOS gate structure, therefore the true electrical response is unknown. Gate area dimensions were kept small due to the long processing times of the focused ion beam deposition tool. Small pads were added at convenient places to probe and provide voltage source and measurement contacts without disturbing the gate electrode which is needed to react with the ambient gas. In Figure 3.1 below, the basic MOS gas sensor design is shown:

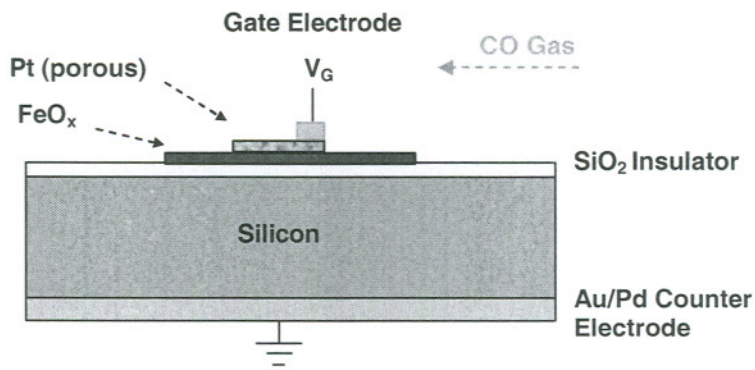

Figure 3.1: Schematic figure of an MOS gas sensor with iron oxide/platinum gate stack

In Figure 3.2 below, a top view of the sensor with a iron oxide modifier film is shown, with the square catalytic Pt gate electrode shown on top of an underlying iron oxide film disk.

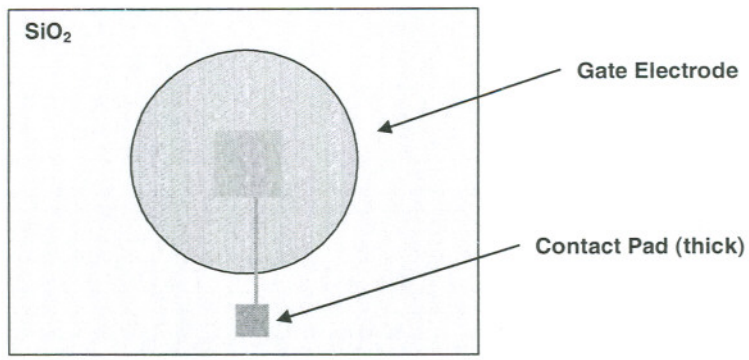

Figure 3.2: MOS gas sensor with iron oxide/platinum gate stack (top view)

Three specific sensor configurations were fabricated and tested and will be referred to as Sensor 1, Sensor 2, and Sensor 3 throughout the remainder of this paper. The specific sensor film dimension specifications are shown in Table 3.1 below.

Table 3.1: Proposed MOS gas sensor design parameters

Property	Sensor 1	Sensor 2	Sensor 3
Pt gate electrode thickness and area	60 nm, 0.01 mm^2	30 nm, 0.01 mm^2	60 nm, 0.01 mm^2
Iron oxide film thickness and area	60 nm, 0.20 mm^2	N/A	N/A
Si sheet resistance (p-type)	10 Ω-cm	10 Ω-cm	10 Ω-cm
Wafer thickness	750 μm	725 μm	725 μm
Oxide thickness	900 nm	7 nm	7 nm
Au/Pd counter-electrode thickness	50 nm	50 nm	50 nm
Pt contact pad thickness and area	1 μm, 0.005 mm^2	1 μm, 0.005 mm^2	1 μm, 0.005 mm^2
Pt contact wire thickness and length	1 μm, 200 μm	1 μm, 200 μm	1 μm, 200 μm

Sensor 1 was fabricated on a p-type silicon chip with a bulk resistivity of 10 Ω-cm and 900 nm thick thermal oxide onto which iron oxide thin film disks were patterned. The iron oxide film was targeted for a thickness of 60 nm to allow CO fast diffusion through to the gate oxide. A Pt gate electrode thickness of 60 nm was chosen based on TEM analysis that

indicated a continuous but highly diffusive small grain structure which would allow analyte gas molecules the ability to reach the iron oxide film quickly. Sensor 2 and Sensor 3 were both fabricated on the same silicon substrate with a thin gate oxide of only 7 nm with Pt metal electrode thicknesses of 30 nm and 60 nm, respectively, as shown below (Figure 3.3). In the Pt only sensors, film thicknesses were chosen based on prior studies that thinner electrodes provide the greatest sensitivity.

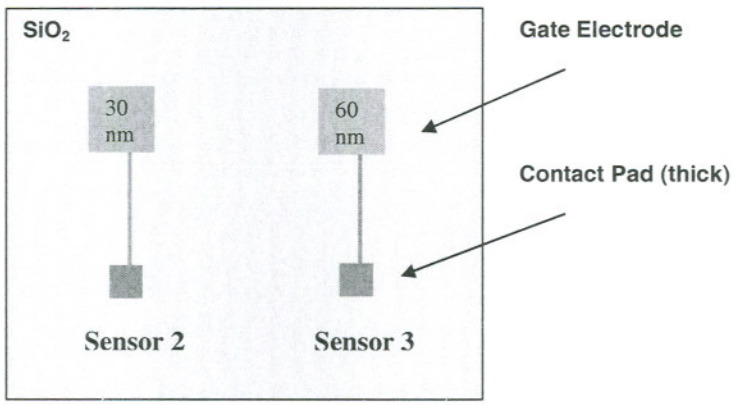

Figure 3.3: MOS gas sensors featuring 60nm and 30nm thin film Pt gates

Operating temperature is an important control feature of most gas sensor designs. Many sensors incorporate integrated on chip inter-digitated heater circuits. In this experiment, an external cartridge heater capable of temperatures up to 200 °C was used, housed in a steel chip mounting platform, with a connected thermocouple to measure approximate surface temperature.

Microfabrication and Analysis

For the fabrication of Sensor 1, p-type (100) silicon fragments of approximately 1 inch square, cleaved from a six inch industrial wafer with an bulk resistivity of 10 Ω-cm were selected. The chip was cleaned using a hydrofluoric acid etch process to remove native oxide and surface contaminants and then a silicon dioxide gate dielectric was grown in a high temperature horizontal diffusion furnace using a thermal dry oxidation process to a thicknesses of 973 to 991 nm. Next, the iron oxide gate areas were prepared for lift-off processing. The wafer surface was first be patterned such that photoresist would coat all non-gate areas and then after metal deposition removed, a chemical solvent could be applied, leaving only areas where iron oxide was in direct contact with SiO_2. A simple mask was designed using Turbo CAD software composed of arrayed circular gate areas 500 microns in diameter and spaced 2000 microns apart to provide room for contact wires and pads (see Appendix A). A glass/chrome mask was fabricated to ensure optimum pattern transfer. Gate areas were patterned using a contact optical photolithography process. The chip was first dehydration baked for 10 minutes at 150 °C. SPR220 positive photoresist was then spun on to obtain a 3 micron thick coating and affixed using HMDS. The coated chip was then soft baked for 1.5 minutes at 115 °C and then processed on the aligner. The photomask was exposed for 60 seconds on a Cobilt/Quinntel Aligner using a 420 nm wavelength Hg lamp light source and 3 micron resolution. Following the exposure step, the pattern was developed using MF-26A Shipley chemical developer for 60 seconds with slight agitation and then hardbaked for 1.5 minutes at 115 °C. Develop checks with an optical microscope revealed roughness around the perimeter of gate film, as seen on prior process runs, but in general well defined gate areas on all samples with a measured diameter of 650 microns.

High current thermal evaporation was used to deposit iron oxide onto the wafer surface. Stoichiometric Fe_2O_3 powder, reddish brown in color was used as the evaporation source material. Fe_2O_3 has a melting and boiling point of 1462 °C. To achieve uniform deposition onto the target at this high temperature, an aluminum oxide (Al_2O_3) coated crucible with a Tungsten wire core was used. The crucible source was filled with a pre-measured amount of iron oxide powder and placed approximately 7 cm from the target. 30 mg of Fe_2O_3 was estimated to achieve a 60 nm thick deposited film based on semispherical evaporation volume from the crucible source, the density of Fe_2O_3, and distance of the crucible from the target. Evaporation was conducted at a belljar pressure of 6×10^{-6} Torr for 20 minutes ramping up to 18 A and 25 V(dc) until all source material was evaporated. Some residue material charred black in color remained in the crucible bowl after processing. Trial and error determined that an amount of 41.8 mg of hematite powder was required to deposit a 60 nm thick film by measuring before and after masses. Following deposition of the iron oxide film, the coated wafer fragments were placed in acetone in a heated ultrasonic cleaner for 5 minutes, rinsed with dionized water, and dried with nitrogen to remove the remaining photoresist and lift off iron oxide outside of the gate areas. The surface was checked under an optical microscope to ensure clean lift-off and existence of gate areas which measured 520 microns in diameter. The deposited oxide film appeared opaque and orange-pink in color.

Focused ion beam (FIB) induced deposition of Pt from a precursor gas of trimethyl platinum was used to deposit the gate electrode films and contact pads and wires. FIB allows patterns to be directly transferred to the wafer surface without lithographic or other indirect printing techniques by scanning a focused beam of gallium ions at a 25 kV accelerating voltage across the surface on which the precursor gas is absorbed. FIB deposited Pt has been shown to produce a metal film with a composition of 46% Pt, 28% Ga, 24% C, and 2% O with a bulk resistivity 7 times greater (70 μΩ·cm) than that of pure Pt [19]. In this experiment, a FEI 610 FIB workstation was used with an extractor voltage of 9.18 kV and ion beam current of 501 pA with a 0.4 μs dwell time at 500X magnification. Pt was deposited in the same pattern for each of the gas sensors fabricated with process times noted in parenthesis: 100 x 100 μm gate electrode area of either 30 or 60 μm in thickness (00:19:14 and 00:38:28 respectively), 50 x 50 μm contact pad of 0.25 μm in thickness

(00:40:24), and a 1 x 400 μm wire of 0.25 μm in thickness (00:03:12). Due to long setup and processing times and pattern point restrictions, Pt area dimensions were restricted and the 100 x 100 μm area was completed in four overlapping 50 x 50 μm square area depositions. The contact wire was also deposited in two phases by overlapping two 200 micron lengths. Figure 4.1 below was a FIB secondary electron image captured at 100X magnification of Sensor 1 just after deposition showing the Pt gate electrode, wire, and contact drawn on top of an iron oxide disk.

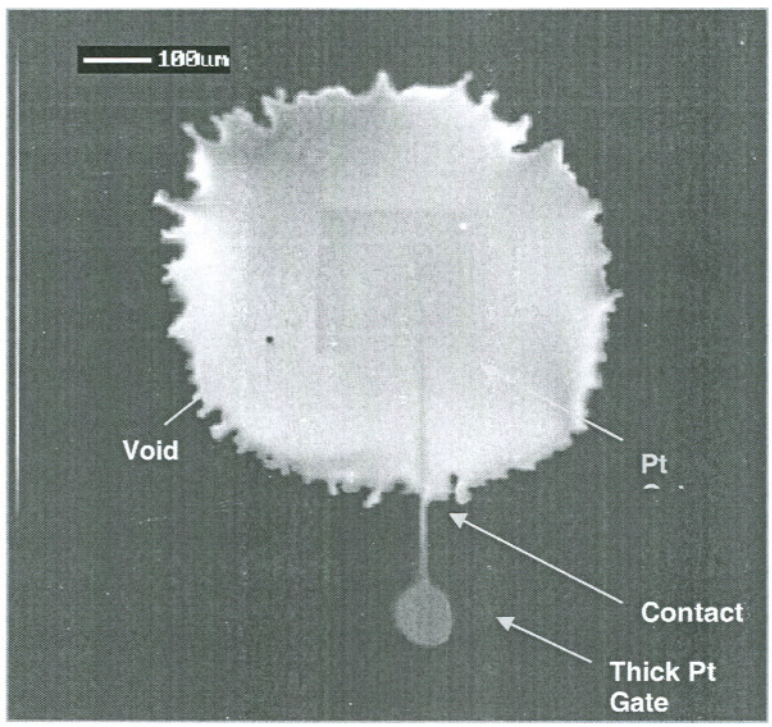

Figure 4.1: FIB secondary electron image of Sensor 1 gate with Pt electrode/contact on iron oxide

The rough edges and peninsulas on the perimeter of the iron oxide film after the lift off processing is clearly evident as are apparent void areas. FIB secondary electron images of Sensor 2 and Sensor 3 were captured at 500X magnification and 45 degree tilt, again showing the Pt gate electrode, wire, and contact (Figures 4.2 and 4.3). In both images, damage areas from ion beam rastering during short imaging periods can be seen.

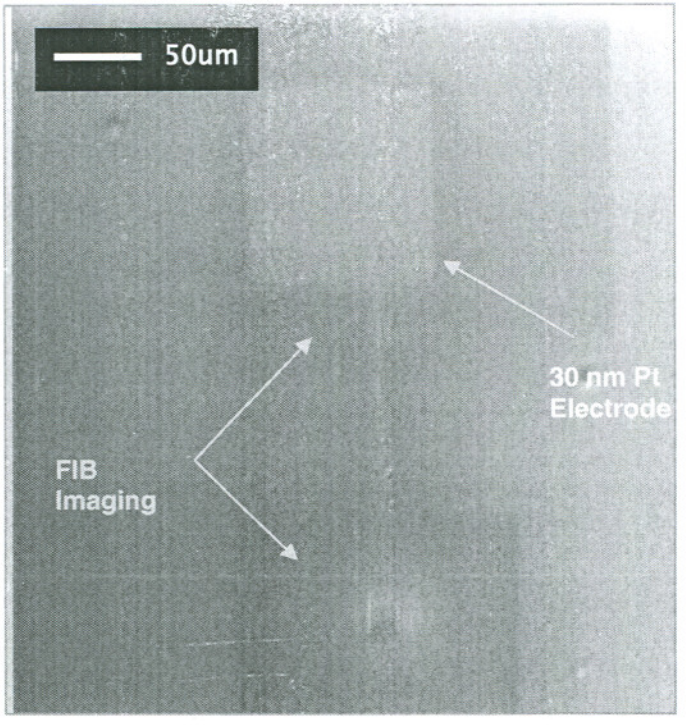

Figure 4.2: FIB secondary electron image of Sensor 2 gate with Pt electrode/contact (500X, 45° tilt)

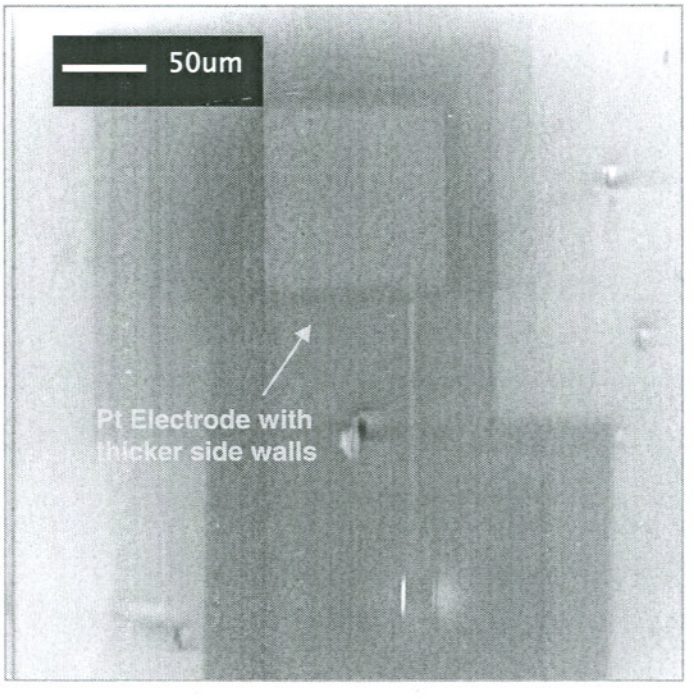

Figure 4.3: FIB secondary electron image of Sensor 3 gate with Pt electrode/contact (500X, 45° tilt)

The 0.25 micron thick gate contact can be clearly be seen with taller side walls than the gate electrode. Also evident is the thicker electrode side walls of Sensor 3 as compared to Sensor 2 as expected. The Pt deposited areas show rounded edges at 500 pA as opposed to more vertical edges seen at smaller beam currents.

To establish a good backside electrical contact for each sensor, a gold palladium film was sputtered using a Technics Hummer II argon plasma sputter coater to produce a thickness of approximately 500 Å. Prior to sputter coating, the sensor backsides were scratched using a diamond scribe to break through any existing silicon dioxide coating to form contact between the Au/Pd and silicon substrate. During testing, the backside is put in direct contact to a solid steel frame where a signal ground wire is connected. A conductive epoxy compound was used to connect fine 3 mil wire to the gate contacts where signal voltage could be applied. The epoxy resin was premixed with a hardener and then coated on a needle point which was then used to apply the epoxy exactly onto the contact area under an optical microscope. Once marked, small wire lengths were affixed to the sensor chips using a glue epoxy compound in close proximity to the contact mark. More conductive epoxy was then applied bonding the wire to the epoxy coated gate contact.

Scanning electron microscope images were taken of all three sensors after fabrication was completed. Figure 4.4 below shows an imaged iron oxide gate area with many void areas as large as 10 microns across present and islands and peninsulas on the perimeter of

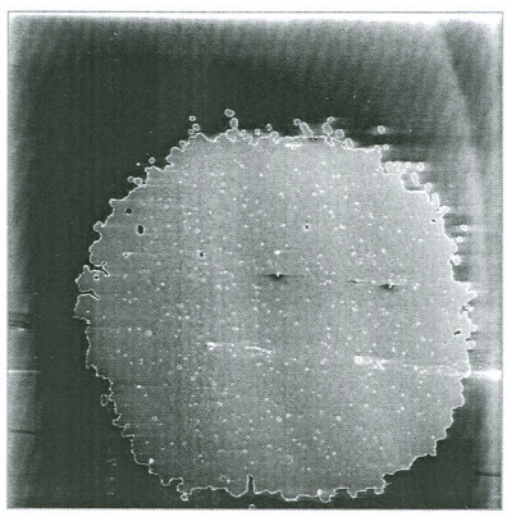

Figure 4.4: Secondary electron image of iron oxide film at 100X magnification, 10 kV accelerating voltage, and no stage tilt

the film. SEM secondary electron images of Sensor 2 and Sensor 3 at an accelerating voltage of 10 kV and 250X magnification are shown below in Figures 4.5 and 4.7. The overlapping 50 micron Pt squares produced by the FIB to construct a larger 100 micron gate electrode can be clearly seen as can the two connecting sections of the contact wire. Charging particles can be seen across the surface of the wafer in both images shown as bright specks.

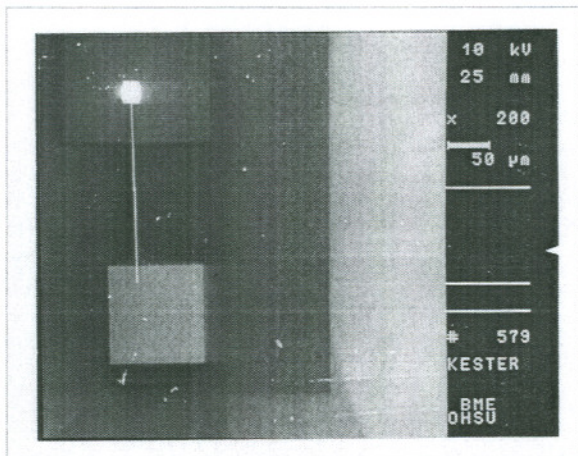

Figure 4.5: SEM secondary electron image of Sensor 2 with 30nm thick Pt gate film at 250X magnification, 10 kV accelerating voltage, and no stage tilt

Stereo pair images of the iron oxide film edges were taken and an actual deposited thickness of 100 nm was estimated with an error of ± 5 nm. Figure 4.6 below shows a view of the oxide edge at a positive 5 degree microscope stage tilt.

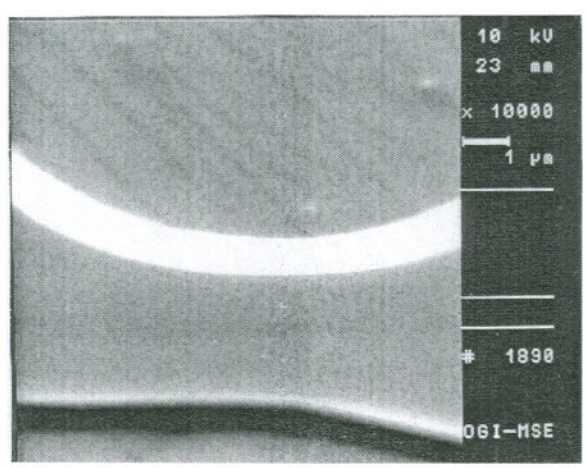

Figure 4.6: SEM secondary electron image of iron oxide edge at 10000X magnification

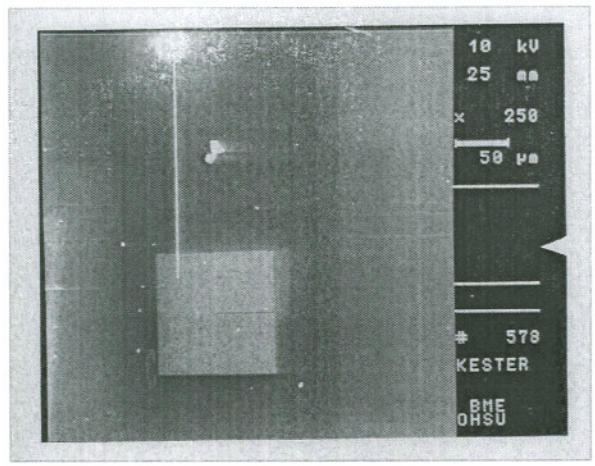

Figure 4.7: SEM secondary electron image of Sensor 3 with 60nm thick Pt gate film at 250X magnification, 10 kV accelerating voltage, and no stage tilt

Transmission electron microscope (TEM) images were obtained for both the Pt and iron oxide films. Film grain sizes were measured and the composition and stoichiometry of the iron oxide film was evaluated. A TEM carbon grid was carefully prepared with FIB deposited Pt bars with thicknesses of 10, 20, 30, 40, 50, and 60 nm. In Figure 4.8 below, the bright field TEM image of a 60 nm thick Pt film is shown with a measured average grain size of 30 Å and more highly diffusive areas, potentially pores, are visible as bright areas. The film is also shown to have a continuous grain network which should provide suitable conductivity as a gate electrode to charge the capacitor.

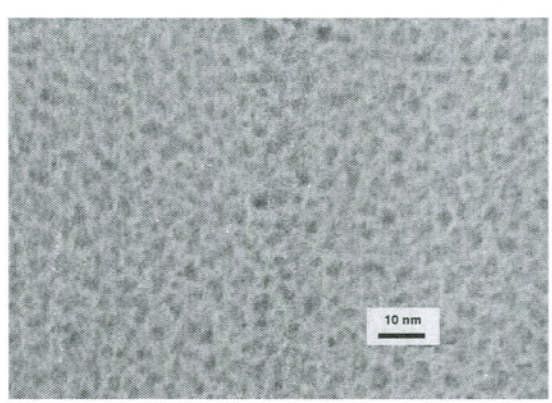

Pt 60nm Film. 200kV Bright Field,
500kX magnification

Figure 4.8: TEM bright field image of 60nm thick FIB deposited Pt film at 500kX magnification

A bright field TEM image of a 30 nm thick Pt film is shown below in Figure 4.9. In this image, smaller grain sizes are measured with an average size of 20 Å and more diffusivity than that of the 60 nm film. However, again enough continuity of the film structure appears to exist to be used as a gate electrode. The 10 and 20 nm films appeared as disconnected networks and therefore were discarded as possibilities for use in a robust sensor design. As shown by Lofdahl et al., catalytic films exhibited effective sensing properities below 400 Å.

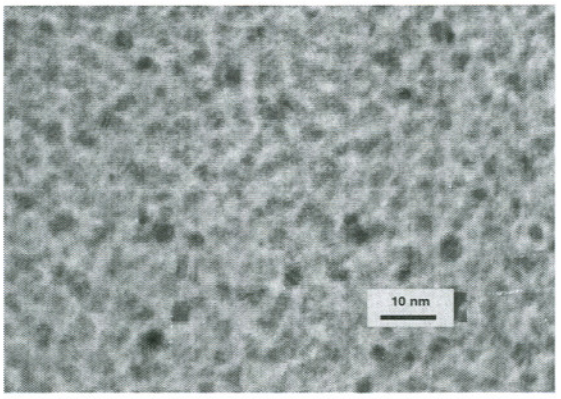

Pt 30nm Film, 200kV Bright Field,
500kX magnification

Figure 4.9: TEM bright field image of 30nm thick FIB deposited Pt film at 500kX magnification

To evaluate the chemical composition and exact stoichiometry of the iron oxide film, TEM diffraction patterns were evaluated and an SEM x-ray analysis was completed. Diffraction patterns of the FIB deposited 30 nm Pt film showed two distinct rings when measuring from the film negative at 20.4 mm and 36.8 mm indicating a compound material as opposed to pure elemental Pt as expected (Figure 4.10). Iron oxide diffraction patterns revealed 8 distinct rings from which translated to physical d-spacings lengths based on a 4.62 Å-cm camera constant (Figure 4.11).

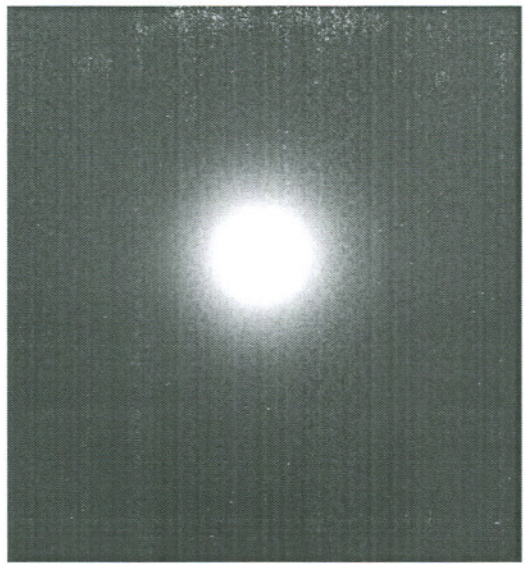

Pt 30nm Film, 2.64Å* camera constant

*4.62Å camera constant on image negative

Figure 4.10: TEM diffraction pattern of FIB deposited 30nm thick Pt film

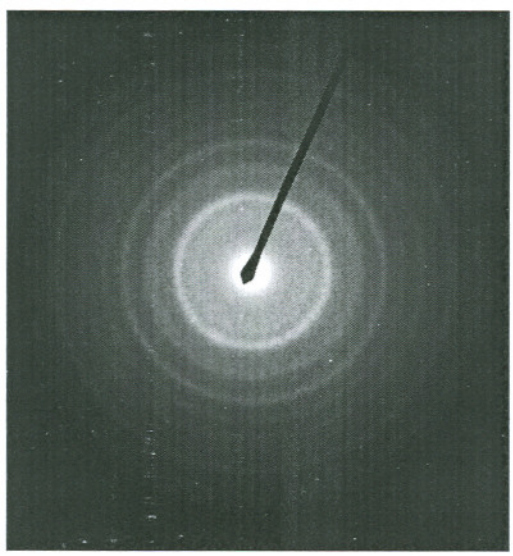

Fe_nO Thin Film, 2.64Å* camera constant

Figure 4.11: TEM diffraction pattern of thermally evaporated Fe_2O_3

The d-spacing measurements shown below in Table 4.1 indicate a closest match to the wustite form of iron oxide, FeO, in face-centered-cubic orientation.

Table 4.1: Measured atomic d-spacings of thermally deposited iron oxide film

Camera constant = 4.62 Å-cm and $2\lambda L = C$

Diffraction ring	d-spacing (Å)
1	2.64
2	2.06
3	1.51
4	1.20
5	1.04
6	0.94
7	0.79
8	0.69

SEM x-ray analysis was conducted on the iron oxide film with a detector setup with the beryllium window removed so that low atomic number elements could be detected. The film stack penetrated by secondary electrons is shown below in Figure 4.12.

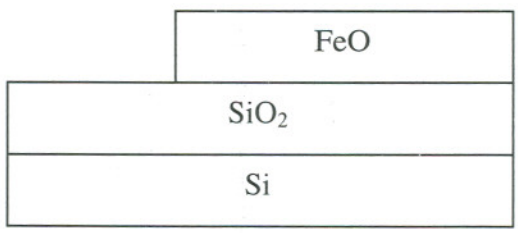

Figure 4.12: Thin film stack analyzed by SEM x-ray detector

A baseline x-ray spectrum, shown below in Figure 4.13, was collected by scanning an area of silicon dioxide near the iron oxide gate film region using an accelerating voltage of 5 kV at 500X magnification. As expected, the captured x-ray spectrum revealed a strong silicon K band peak at 1.739 keV and a weaker oxygen K band peak at 0.525 keV.

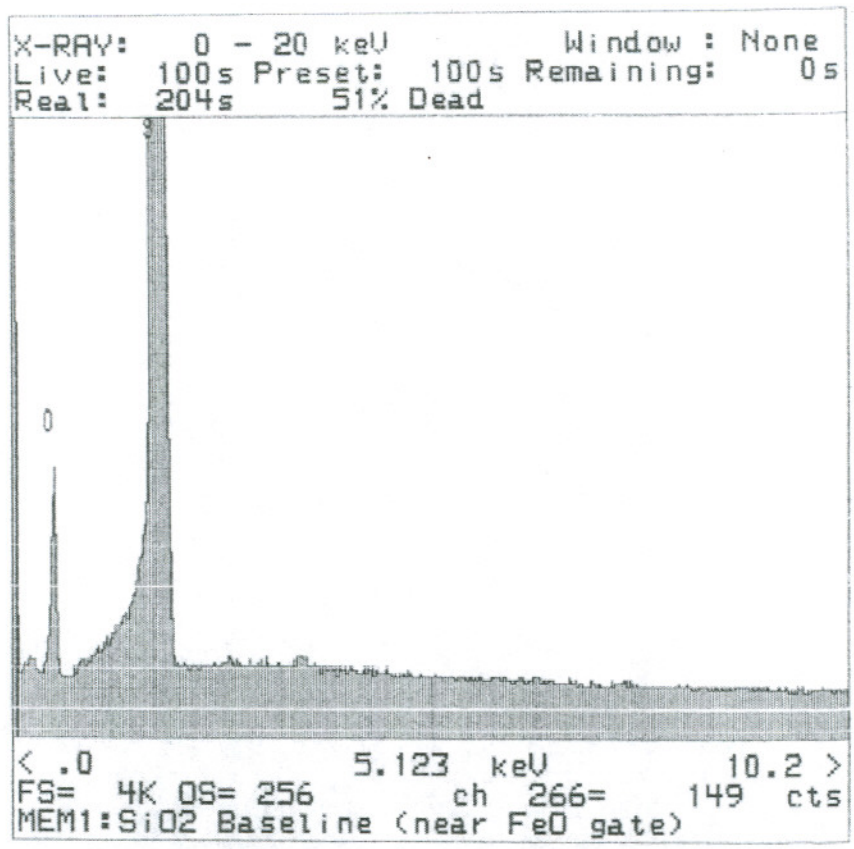

Figure 4.13: X-ray spectrum detected scanning surface area near iron oxide film

A second spectrum was captured scanning the actual iron oxide area at the same accelerating voltage and magnification. In Figure 4.14 below, a strong silicon K band peak is again present and a stronger oxygen K band peak is seen as compared against the baseline measurement. Iron K alpha and beta bands can be clearly seen at 6.391 keV and 7.508 keV. Further, aluminum K band and tungsten L band spectra are found at 1.486 keV and 7.388 keV, 8.398 keV, and 9.673 keV respectively, likely caused by some decomposition of the AlO coated crucible and tungsten filament during the evaporation process. An exact Fe to O ratio was difficult to determine from the compositional analysis as the electron beam also penetrated into the silicon dioxide and silicon bulk layers as evident by the intense silicon peak.

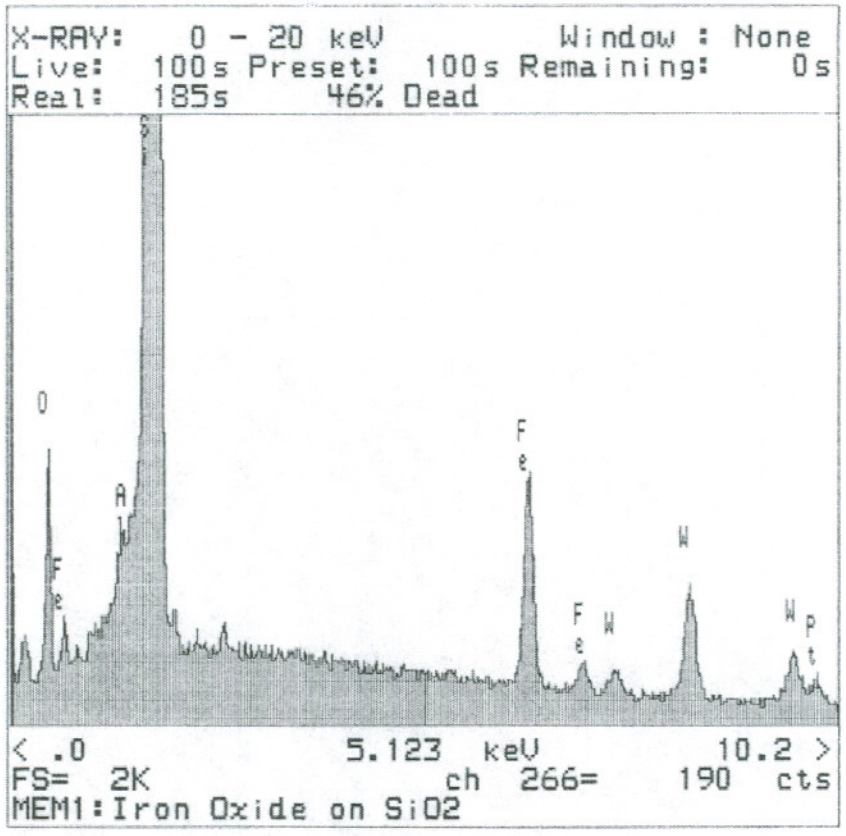

Figure 4.14: X-ray spectrum detected scanning surface of iron oxide film

Results and Discussion

The performance of a gas sensor is determined based on its response time in detecting presence, recovery time of the sensor once the analyte gas is removed from the ambient, sensitivity to analyte gas concentration, and the ability of the sensor to discriminate between the gas to be sensed and other gases present in the ambient environment. Sensors described in this experiment were evaluated for sensitivity to low analyte gas concentrations, the effect on response due to increase of the operating temperature, and their recovery behavior to determine if the sensor-gas chemical reaction was a chemisorption or physisorption process. The sensors are only evaluated in their ability to detect carbon monoxide at low concentrations, however it is believed that detection of any gases known to respond to Pt and iron oxide based gates as shown in prior experiments would also be realizable. The response of each sensor to carbon monoxide gas exposure was evaluated by exposing the MOS gate structures to increasing concentrations of carbon monoxide gas mixed in dry air (20% oxygen) at constant normal pressure and at room temperature and 200 °C. A gas flow test system was constructed consisting of a 1.5 L sealed glass chamber, calibrated flow meters to the measure incoming gas flow, and a wet test meter to measure the total flow rate exhausted from chamber (Figure 5.1). To obtain a 200 °C operating temperature, heat was applied by a cartridge heater plumbed into a specially designed aluminum sensor chip holder. Temperature was measured and controlled by an Omega HH12 digital temperature gauge and thermocouple and variac heat source. The electrical properties and gas response were evaluated by measuring capacitance-voltage (C-V) characteristics obtained from an HP 4275A Multi-Frequency LCR Meter and HP Vee CV measurement software. Gate voltage signals were swept from negative to positive with a frequency of 1 MHz. Signal probes were connected to wires soldered directly to the epoxied

gate contact wires on the sensor chip and a signal ground wire was connected to the chip holder.

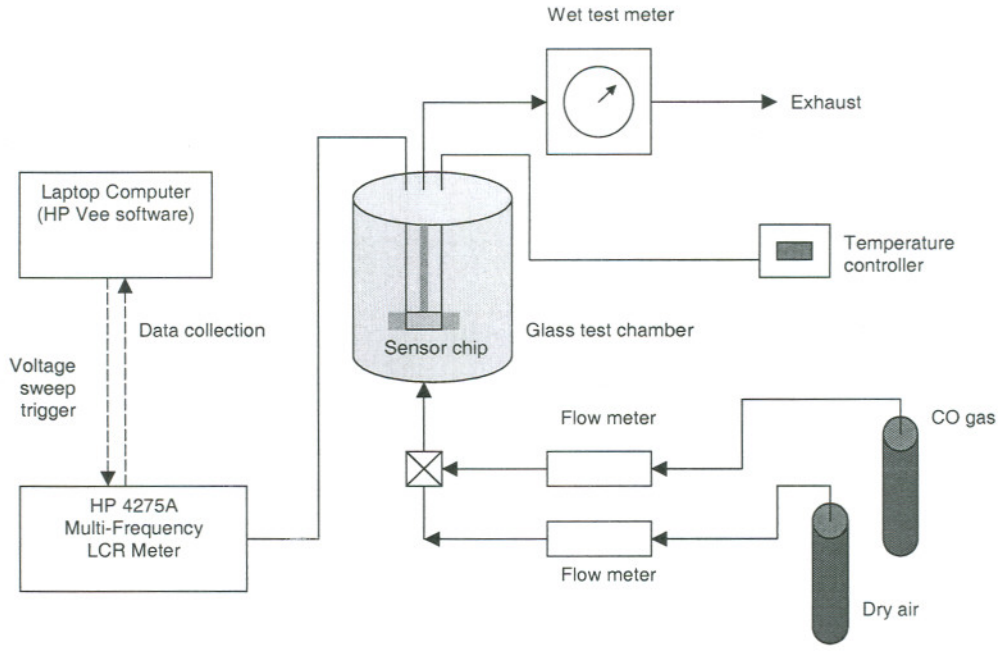

Figure 5.1: Schematic of carbon monoxide gas detection system

Figure 5.2: Digital photograph of lab setup for gas exposure testing

The metal backside of the chip was put in contact to the aluminum holder and held firmly with a tightened spring clip. Figure 5.2 above shows the actual lab setup for the gas exposure testing conducted. The wet test meter and exhaust hood can be seen in the foreground with the exposure test chamber slightly behind and to the right. The C-V control computer and LCR meter are located on the far right. In Figure 5.3 below, CO gas and air flow tubes can be seen entering the test chamber from bottom and heater control and thermocouple wires, electrical signal conductors, and exhaust tube can be seen entering and exiting the chamber, respectively from above.

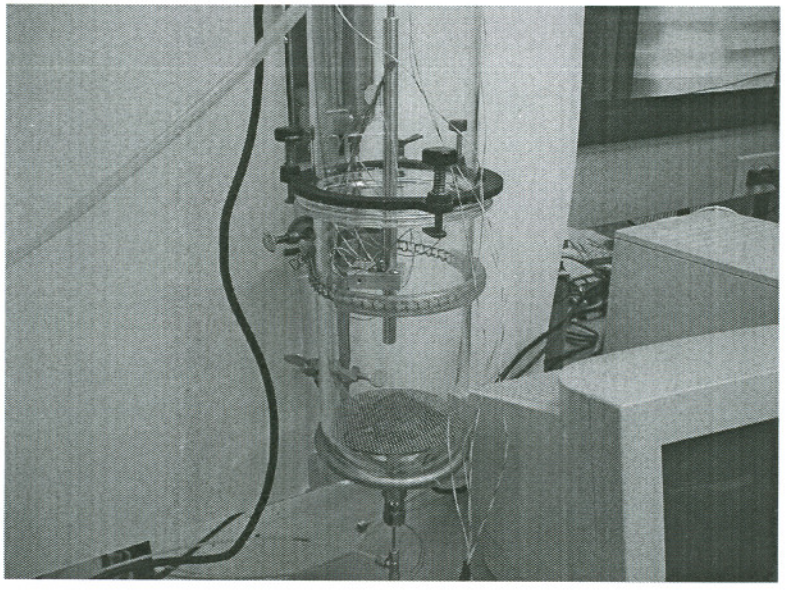

Figure 5.3: Gas exposure test chamber lab setup

Below, the carbon monoxide gas and dry air source bottles, control valves, and flow meters are shown (Figure 5.4).

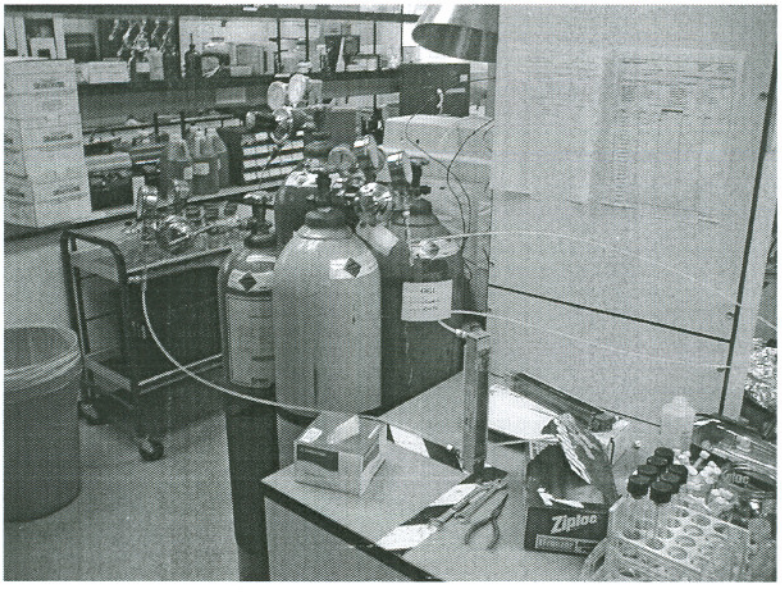

Figure 5.4: Carbon monoxide gas and dry air bottles and flow meter lab setup

Prior to applying the conductive epoxy for external connections during gas exposure testing, the sensor chips were tested on an electrical probe station with a connected LCR meter to obtain device baseline high frequency C-V responses at room temperature. Sensor 1, 2, and 3 were probed along with a pre-fabricated C-V test disk with a 500 nm thick Al/Cu gate electrode film 500 microns in diameter. A 60 nm Pt gate contact was deposited by the FIB on this Al/Cu area as well prior to testing. Sensor 2 and 3 C-V measurements revealed high frequency plots characteristic for p-type MOS devices with accumulation in the negative voltage region and depletion in the positive voltage regions with no inversion and flat band voltages shifted slightly negative than zero as shown below in Figure 5.5.

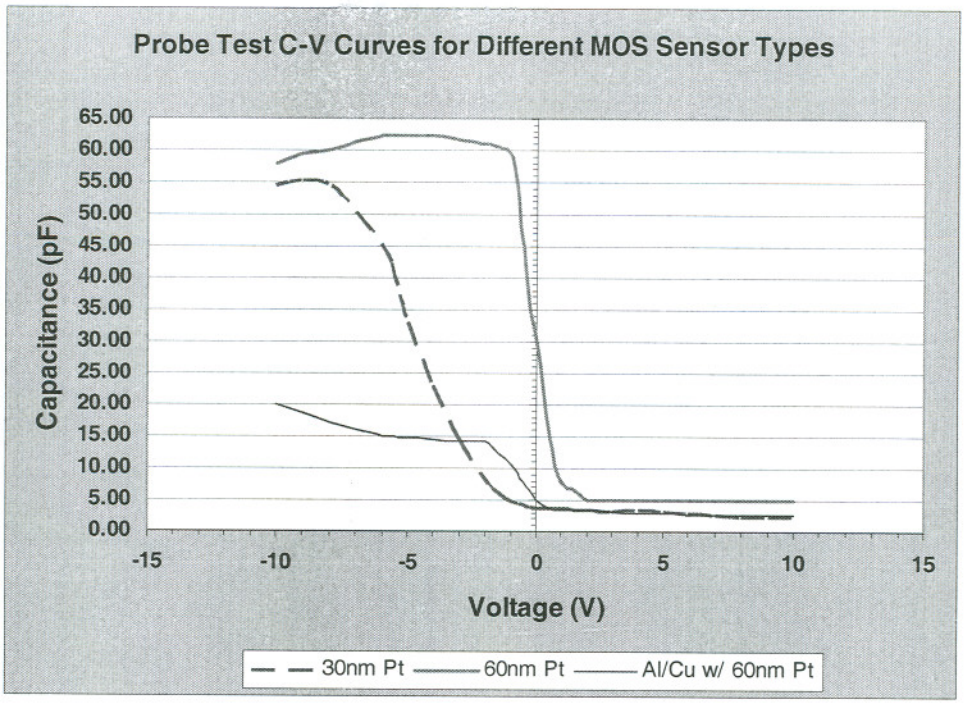

Figure 5.5: Electrical prober C-V characteristic curves of Sensor 2, Sensor 3, and pre-existing Al/Cu CV disk with deposited 60 nm thick Pt film

However, Sensor 1 demonstrated no capacitor charging response with no visible accumulation or depletion to a voltage sweep of -/+ 35 V at 1 MHz, responding with a static capacitance value of 3.89 pF. It was believed that due to the relatively large thermal oxide thickness of 900 nm and estimated theoretical breakdown voltage of 900 V that a larger applied gate voltage was required. An external voltage source capable of driving up to ±200 V was attempted, resulting in catastrophic punch-through and breakdown as shown in the images below (Figures 5.6 and 5.7). Imperfections in the Pt film and Pt/oxide interface caused during the ion deposition process are believed to be the root cause of the failure.

.

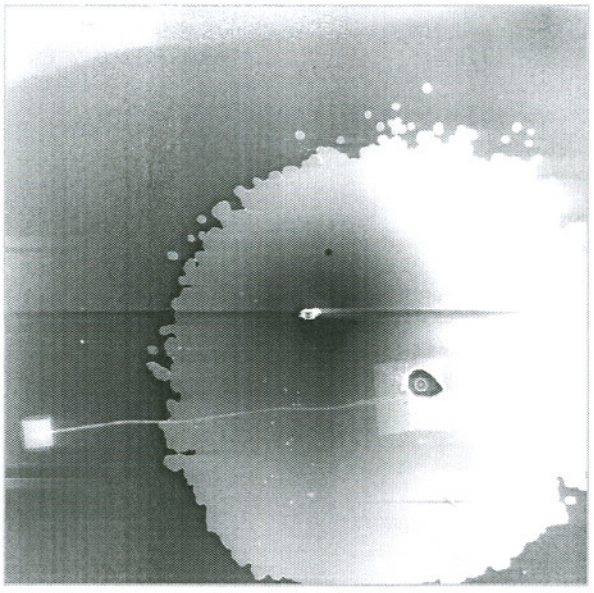

Figure 5.6: SEM image of gate area where breakdown destruction can be clearly seen

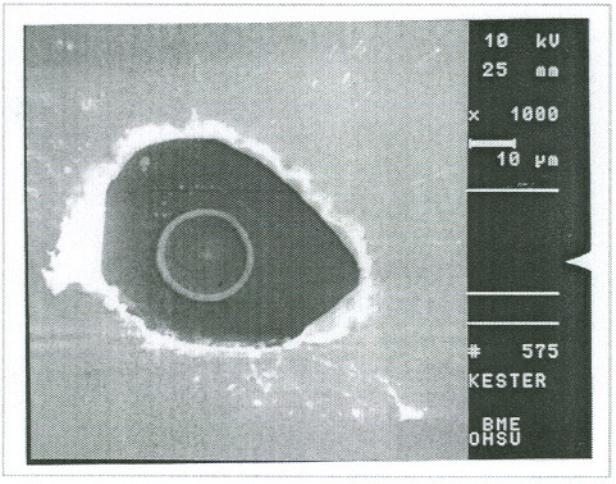

Figure 5.7: SEM close up image of breakdown destruction area

Gas testing was conducted by establishing a constant background flow rate, initially of dry air, of 1000 mL/min. The sensor was exposed at room temperature to a constant concentration of CO gas in 10 minute long intervals spaced 10 minutes apart from finish to

start to allow the sensor thin film trapped charge states to come back equilibrium (see Appendix B for gas exposure test procedure). It was expected that if the reaction was in fact a chemisorption process then the flat-band voltage would not return to its initial baseline value established at a 0 ppm CO concentration. The carbon monoxide source was 1000 ppm true CO concentration in a dry air 20% oxygen mix volume. This source gas was mixed with a second dry air source to produce CO concentrations of 0, 25.3, 47.6, 90.9, 200.0, 411.8, 500.0, 800.0, and 1000.0 ppm. Room temperature tests of Sensor 2 revealed detectable positive voltage shifts of 200 mV at CO concentrations of 25 ppm and 1.25 V at 1000 ppm. Sensor 3 demonstrated positive voltage shifts of 150 mV for 25 ppm CO and 490 mV at 1000 ppm.

Table 5.1: Flat band voltage shifts measured for Sensor 2 and Sensor 3 exposed to CO gas

Voltage sweep -/+ 10V at 1 MHz

CO concentration (ppm)	Sensor 2 (mV)	Sensor 3 (mV)	Total flow rate (mL/min)
0	-	-	1000
25.3	200	150	1026
47.6	700	480	1050
90.9	1100	300	1100
200.0	750	350	1250
411.8	650	380	1700
500.0	950	580	2000
800.0	1200	530	1250
1000.0	1250	490	1000

The Sensor 2 MOS capacitor flat band voltage was estimated at 81.80 pF at –0.8 V at 0 ppm CO. Sensor 2 exhibited responses at every concentration level and voltage shift drops during settling periods. At the 50 ppm concentration level there was a sharp positive shift with very little drop off and at the 100 ppm concentration level the sensor behaved as though trap sites became saturated nearly reaching the peak shift seen at 1000 ppm (Figure 5.8). Figure 5.9 shows the actual C-V response seen at each CO concentration level revealing detectable voltage shifts at each level as compared to the 0 ppm level. The capacitance drop off in the accumulation band was suspected to be caused by possible oxide

breakdown. The applied voltage exceeded the theoretical breakdown voltage, which was estimated at 7 V for the oxide assuming a 10 MV/cm field strength for thermal oxide.

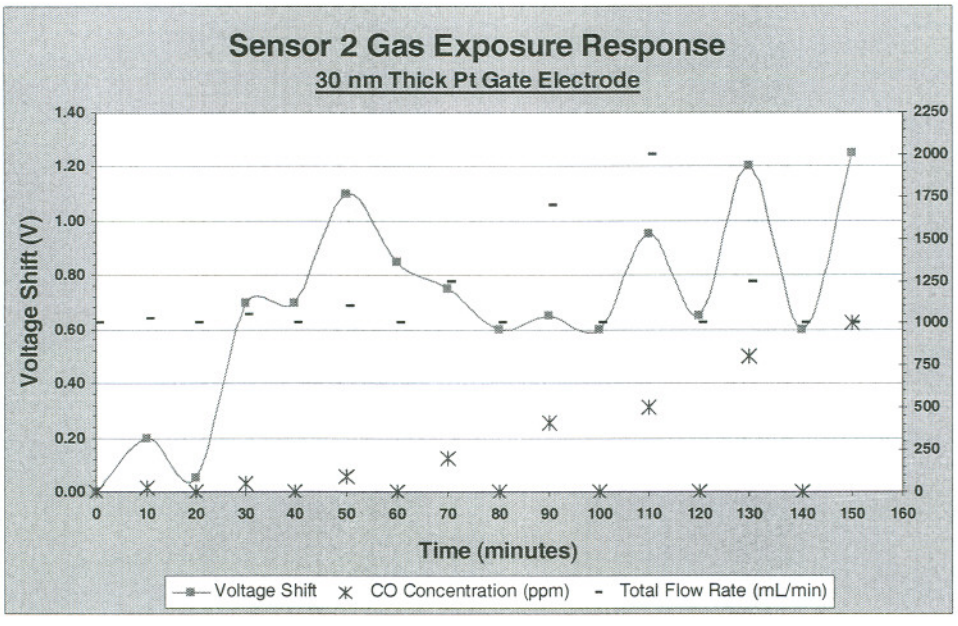

Figure 5.8. Sensor 2 voltage shift response over complete CO concentration test cycle

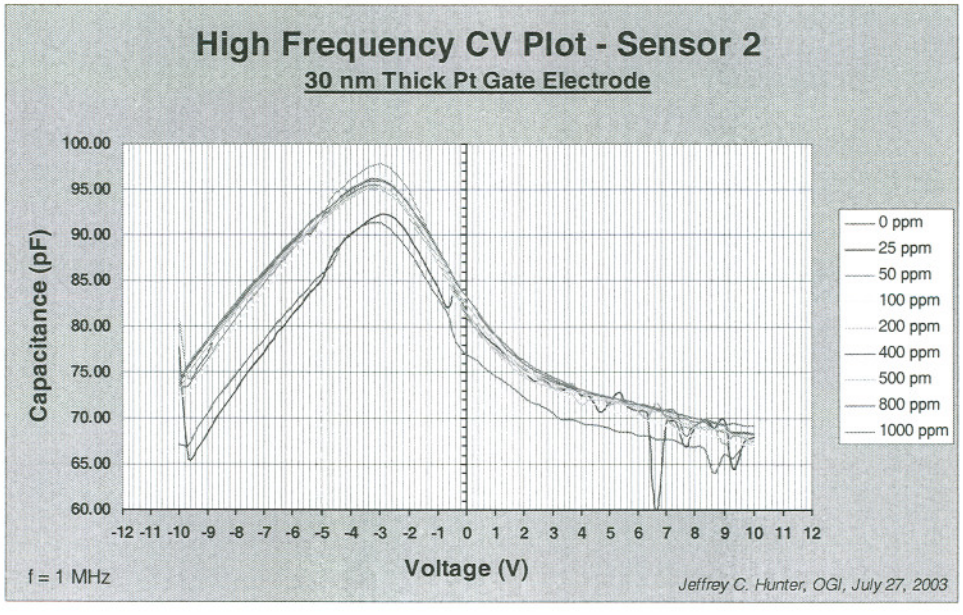

Figure 5.9: Sensor 2 high frequency C-V response at different CO gas concentration exposures

A second measurement was made on a second 30 nm sensor fabricated on the same substrate. C-V measurements made on this sensor revealed a similar voltage shift response but without the drop off in the accumulation region (Figure 5.10).

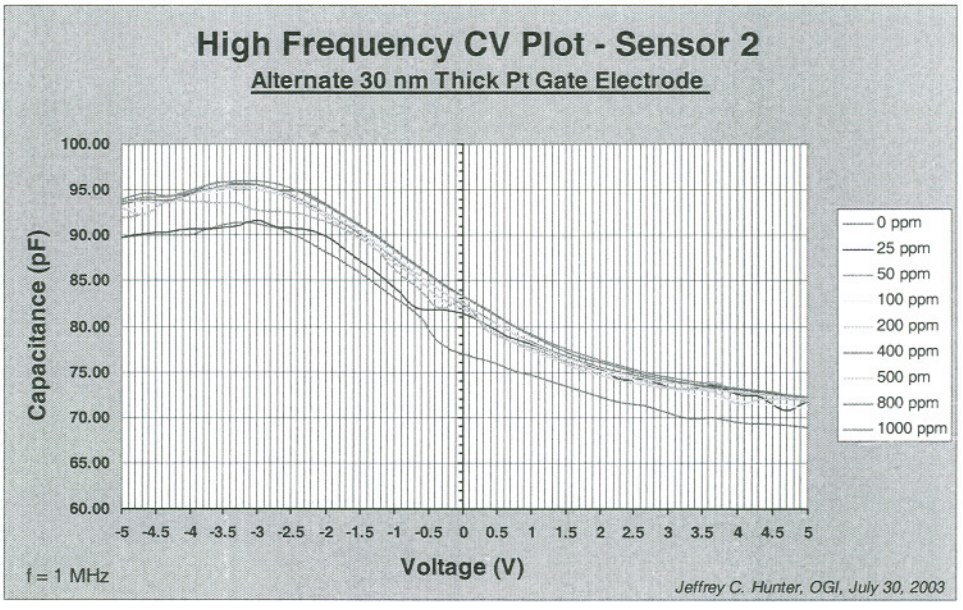

Figure 5.10: Sensor 2 high frequency C-V response over -/+ 5 V sweep at different CO gas concentration exposures

Sensor 3 with its 60 nm thick gate film exhibited smaller voltage shift responses at the same concentrations. It is believed that the porosity of the FIB deposited 30 nm film was optimized and provided more surface trap sites for charges than the 60 nm film. The C-V response of Sensor 3 revealed a second knee moving into the flat-band and depletion regions likely due to a pronounced parallel capacitance effect of the gate epoxy contact however voltage shifts at each concentration level are evident (Figure 5.11). Figure 5.12 below clearly shows the recovery behavior of the sensor and indicates a chemisorption reaction process as the flat band voltage does not return to zero concentration levels. Even one hour after gas exposure the sensor flat band capacitance of 102.67 pF was shifted by 350 mV as compared to the original 1.00 V measurement.

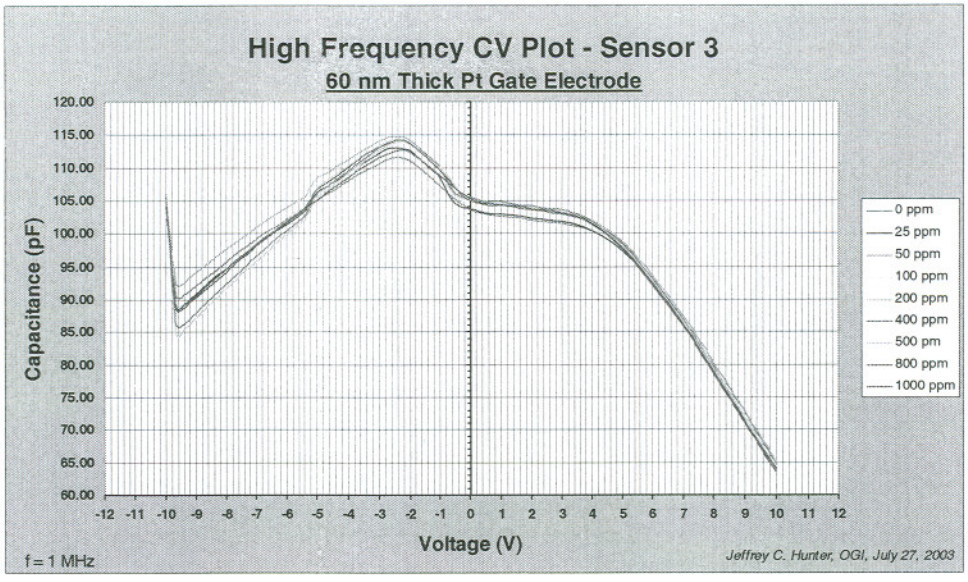

Figure 5.11: Sensor 3 high frequency C-V response at different CO gas concentration exposures

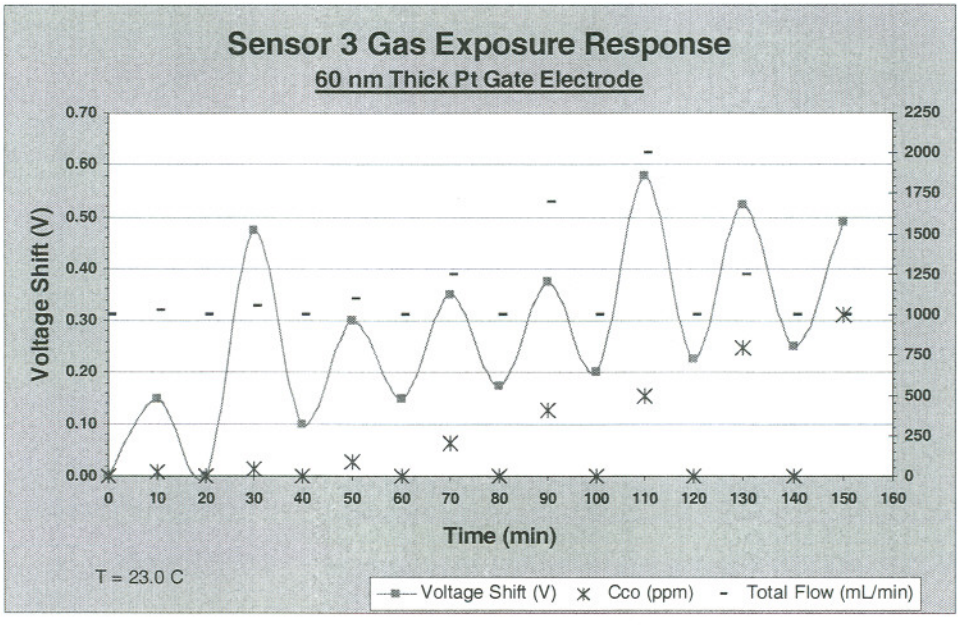

Figure 5.12: Sensor 3 voltage shift response over complete CO concentration test cycle

As expected from baseline probing results, Sensor 1 demonstrated a static capacitance response when swept with -/+ 35 V at 1 MHz and no voltage shift based on

baseline C-V tests. Sensor 1 was only evaluated at CO concentrations of 0 ppm and 1000 ppm following the same exposure intervals as Sensor 2 and Sensor 3 tests. A change in capacitance magnitude of 6.5 pF is evident across the applied gate voltage range as the sensor is exposed to 1000 ppm CO indicating a change in the bulk conductivity (Figure 5.13).

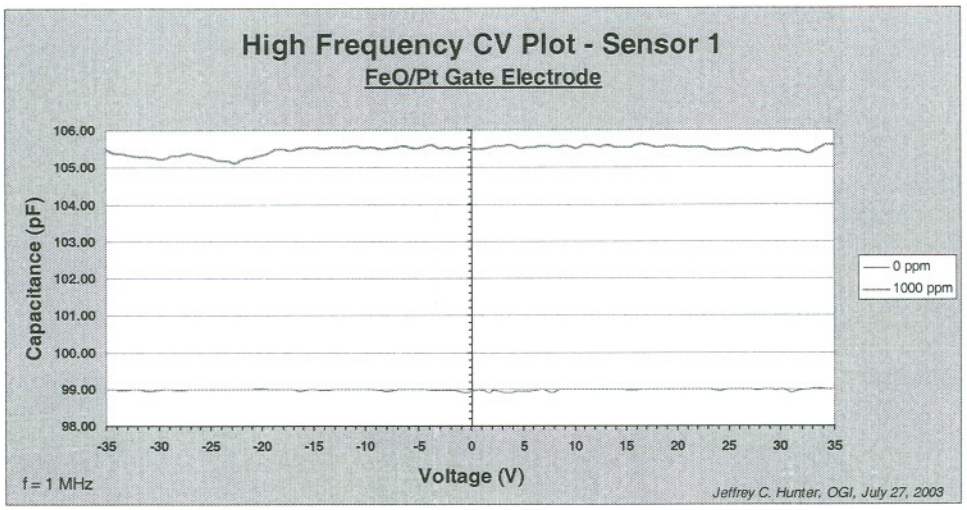

Figure 5.13: Sensor 1 high frequency C-V response over -/+ 35 V sweep at different CO gas concentration exposures

Table 5.2: Measured Sensor 1 static capacitance during CO gas exposure

Voltage sweep -/+ 35V at 1 MHz

CO concentration (ppm)	Avg. capacitance (pF)	Total flow rate (mL/min)
0	98.95	1000
1000	105.51	1000

A second gas response test was conducted raising the operating temperature to 200 °C by increasing the variac heater to 70% at 140 V. Significant upward shifts in capacitance were seen in the C-V response of each sensor type and low frequency response characteristics appeared as inversion carriers are able to respond with the added thermal energy [16]. At 200 °C the shape of the C-V response curves change at 0 ppm and 1000

ppm and it was difficult to determine an accurate flat band shift. For Sensor 2, a change in capacitance of 27 pF at an applied voltage of 1.0 V between 0 ppm and 1000 ppm alludes to a dramatic shift. Further investigation of the sensor electrical responses at higher temperatures is required to establish the true response characteristics particularly the affect of temperature on the conductive epoxy connection. Sensor 1 experienced an overall capacitance increase of 24 pF at 0 ppm CO at 200 °C but only a 4 pF change when exposed to 1000 ppm CO.

Table 5.3: Sensor 1 and Sensor 2 capacitance and voltage shift responses during CO gas exposure at 200°C

Voltage sweep -/+ 10V at 1 MHz

CO concentration (ppm)	Sensor 1 Zero volt capacitance (pF)	Sensor 2 Zero volt capacitance (pF)
0	122.41	151.20
1000	118.52	123.01

Conclusion

The stand-alone FIB deposited 30 nm and 60 nm thick platinum sensors demonstrated appreciable voltage shift responses of 200 mV and 150 mV at room temperature in detecting the presence of 25 ppm carbon monoxide. The 30 nm platinum electrode achieved sensitivity to 100 ppm CO of 1100 mV, an order of magnitude greater response than that seen by the Pt/SnOx sensor evaluated by Kasama et. al [18]. Finer grain sizes and increased film diffusivity shown through TEM characterization indicate improved ability of the 30 nm sensor to trap charges during CO exposure reactions as compared to the 60 nm sensor. Selectivity of the FIB deposited Pt film in detecting various gases will need to be evaluated in the future. Further, more characterization of these sensors under higher temperature operation is needed to optimize gas desorption and sensor recovery.

True MOS C-V responses were unable to be obtained from the Pt/iron oxide multi-layer gate construction, however changes in bulk conductivity of electrical charge were evident based on changes in static capacitance values of 6.5 pF at 1000 ppm. Inability of the $Pt/FeO/SiO_2/Si$ capacitor stack to accumulate charge may be due to poisoning of the iron oxide film by gallium ions during the FIB milling/deposition process. It is unclear whether the FeO film deposited would perform as well as the more proven hematite form used in other sensor designs, which could be better achieved through a sputtering process. Further, the iron oxide film although well adhered to the underlying silicon dioxide layer, was unable to produce a stack capable of accumulating and depleting charge fed by minority carriers in the doped substrate. Another approach would be to coat the Pt electrode with iron oxide as a surface modifier detection mechanism and leaving an area for direct metal to metal electrical connection for the gate voltage to achieve a typical MOS C-V response. In future sensor fabrication, passivation and isolation of the gate area contact should be considered and proven connection methodologies such as ball bonding should be employed to remove

any response affects due to this added parallel capacitance and unwanted material reaction effects possibly seen with conductive epoxies. Finally, future solid state gas sensor designs could be extended to a full MOSFET with an exposed gate electrode, which can be integrated into an arrayed multi-sensor system and analysis circuitry.

References

[1] K. Lundstrom, M. Shivaraman, and C. Svensson, "A hydrogen sensitive Pd-gate MOS transistor," *J. Appl. Phys.,* vol. 46, pp. 3876-3881, 1975.

[2] Physics, Chemistry and Technology of Solid State Gas Sensor Devices, Chemical Analysis Volume 125. A. Mandelis, C. Christofides. John Wiley & Sons Inc., New York, 1993.

[3] I. Lundstrom, L. Petersson, "Chemical sensors with catalytic metal gates," *J. Vac. Sci. Technol. A,* vol. 14, no. 3, pp. 1539-1545, May 1996.

[4] D. Filippini, L. Fraigi, R. Aragon, U. Weimar, "Thick film Au-gate field-effect devices sensitive to NO_2," *Sensors and Actuators B, Chemical*, vol. 81, pp. 296-300, 2002.

[5] E. Comini, V. Guidi, C. Frigeri, I. Ricco, G. Sberveglieri, "CO sensing properties of titanium and iron oxide nanosized thin films," *Sensors and Actuators B, Chemical*, vol. 77, pp. 16-21, 2001.

[6] E. Comini, M. Ferroni, V. Guidi, G. Gaglia, G. Martinelli, G. Sberveglieri, "Nanostructured mixed oxide compounds for gas sensing applications," *Sensors and Actuators B, Chemical*, vol. 84, pp. 26-32, 2002.

[7] D. Filippini, T. Weib, R. Aragon, U. Weimar, "New NO_2 sensor based on Au gate field effect devices," *Sensors and Actuators B, Chemical*, vol. 78, pp. 195-201, 2001.

[8] K. Kasama, H. Fukuda, S. Nomura, "Highly sensitive MOSFET gas sensors with porous Pt-SnO_x gate electrode for CO gas sensing applications," *Electronics Letters*, vol. 34, no. 14, pp. 1393-1395, July 9, 1998.

[9] M. Lofdahl, M. Eriksson, M. Johansson, I. Lundstrom, "Difference in hydrogen sensitivity between Pt and Pd field-effect devices," *J. Appl. Phys.,* vol. 91, no. 7, pp. 4275-4281, 2002.

[10] J. F. Chang, H. Kuo, I. Leu, M. H. Hon, "The effects of thickness and operation temperature on ZnO:Al thin film CO gas sensor," *Sensors and Actuators B, Chemical*, vol. 84, pp. 258-264, 2002.

[11] M. Lofdahl, C. Utaiwasin, A. Carlsson, I. Lundstrom, M. Eriksson, "Gas response dependence on gate metal morphology of field-effect devices," *Sensors and Actuators B, Chemical*, vol. 80, pp. 183-192, (2001).

[12] A. Abom, E. Comini, G. Sberveglieri, L. Hultman, M. Eriksson, "Thin oxide films as surface modifiers of MIS field effect gas sensors," *Sensors and Actuators B, Chemical*, vol. 85, pp. 109-119 (2002).

[13] Regulations (Standards – 29CFR), Carbon monoxide. – 1917.24. U.S. Department of Labor, Occupational Safety & Health Administration. Available at: http://www.osha.gov/. [Viewed: March 2, 2003].

[14] G. Neri, A. Bonavita, S. Galvagno, P. Siciliano, S. Capone, "CO and NO_2 sensing properties of doped-Fe_2O_3 thin films prepared by LPD," *Sensors and Actuators B, Chemical*, vol. 82, pp. 40-47, 2002.

[15] Lange's Handbook of Chemistry, 13th Ed., J. A. Dean, McGraw-Hill, New York, 1985.

[16] Semiconductor Material and Device Characterization, 2nd Ed., D. Schroder, John Wiley & Sons, Inc., New York, 1998.

[17] Micromachined Transducers Sourcebook, G. T. A. Kovacs. WCB/McGraw-Hill, Boston, MA, 1998.

[18] Chemistry, The Central Science, 4th Edition, T. Brown, H. E. LeMay, Jr. Prentice Hall, Englewoods Cliff, NJ, 1988.

[19] T. Tao, J. Ro, J. Melngailis, "Focused ion beam induced deposition of platinum," *J. Vac. Sci. Technol. B*, 8, (6), pp. 1826-1829, (1990).

Appendix A. Iron Oxide Gate Mask for Sensor 1

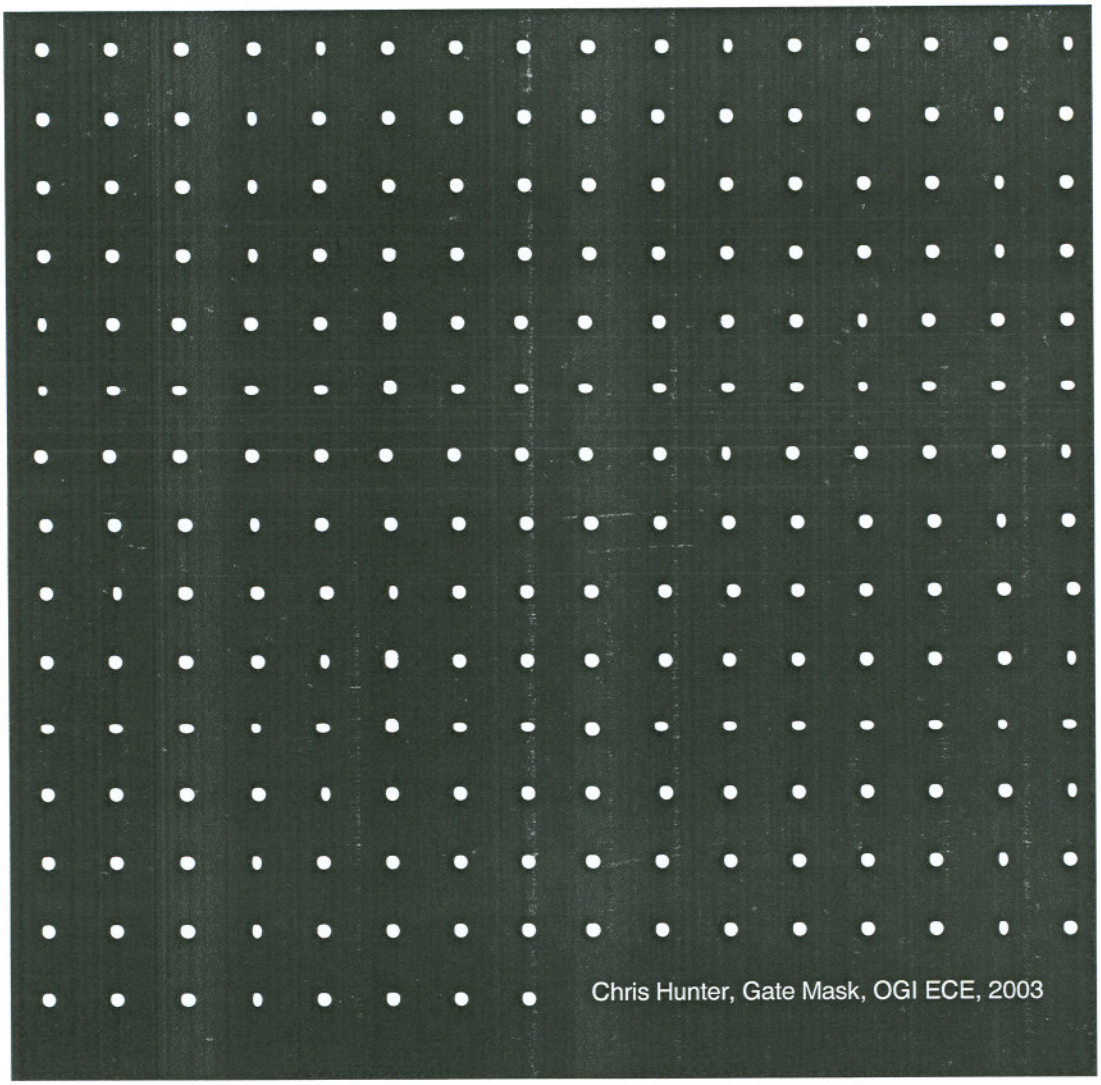

Appendix B. Gas Exposure Test Procedure

Test Conditions:
T = 22.7 C
f = 1 MHz, zeroed
OSC level = 0.6 x 1 V
Exposure pulse: 10 min exposure, 10 min settling time
Bias voltage sweep of -10 to +10 V (Sensor 2 and 3) and -35 to 35 V (Sensor 1); 60 pts collected in .dat files
File names: sensXCY.dat
Initial flow rate of 1000 mL/min of Dry Air

Variables:
Approximate CO gas concentration (ppm): 0, 25, 50, 100, 200, 400, 500, 800, 1000

Procedure:
1) Set the constant background flow rate (Air or CO)
2) Zero voltage
3) Start gas flow at desired flow rate and concentration
4) Start clock for 10 min countdown
5) After 10 min, sweep bias voltage, record Vfb, record capacitance at V=0 and V=Vfb (exposed mode)
6) Record operating temperature
7) Zero voltage
8) Close valve to shut off gas
9) Start clock for 10 min countdown
10) After 10 min, sweep bias voltage, record capacitances and voltages (settled mode)
11) Record operating temperature
12) Zero voltage
13) Return to Step 3

Appendix C. Gas Exposure Test Apparatus

Gas/CV Response Test Apparatus:
CO tank of 1000ppm in dry air solution
Dry air for background
Flow meter 0-1700 mL/min calibrated
Flow meter 0-258 mL/min calibrated
Wet test meter (measuring total flow, exhaust from system) - precision calibrated
Glass test chamber
Variac heater
Aluminum chip holder stand
Cartridge heater
Thermocouple wire
Omega HH12 digital temperature gauge
Exhaust system
CV analyzer software - HP Vee
HP 4275A Multi-Frequency LCR Meter
Tektronics CDM250 Digital Multi-meter
Conductive epoxy
Glue epoxy
Small gauge wire

Appendix D. Carbon Monoxide Exposure Test Data

Test 1 Measurements (Sensor 2):

Elapsed Time (min)	Bias V=0 C (pF)	Voltage Shift	Est. Cfb (pF)	CO Concentration (ppm)	Air Flow Rate (mL/min)	CO Flow Rate (mL/min)	Total Flow Rate (mL/min)	Test Condition	Substrate Actual T (°C)
0	78.77	0.00							22.7
0	77.02	0.00	81.80	0.0	1000	0	1000	settle	22.7
10	81.40	0.20	81.80	25.3	1000	26	1026	exposure	22.7
20	79.10	0.05		0.0	1000	0	1000	settle	22.7
30	81.10	0.70	81.80	47.6	1000	50	1050	exposure	22.7
40	81.11	0.70		0.0	1000	0	1000	settle	22.9
50	83.06	1.10	81.80	90.9	1000	100	1100	exposure	22.9
60	81.63	0.85		0.0	1000	0	1000	settle	23.0
70	81.62	0.75	81.80	200.0	1000	250	1250	exposure	23.0
80	81.14	0.60		0.0	1000	0	1000	settle	23.1
90	82.42	0.65	81.80	411.8	1000	700	1700	exposure	23.1
100	83.31	0.60		0.0	1000	0	1000	settle	23.1
110	82.43	0.95	81.80	500.0	1000	1000	2000	exposure	23.0
120	82.61	0.65		0.0	1000	0	1000	settle	23.0
130	83.28	1.20	81.80	800.0	250	1000	1250	exposure	23.0
140	82.53	0.60		0.0	1000	0	1000	settle	23.0
150	83.30	1.25	81.80	1000.0	0	1000	1000	exposure	23.0

Test 2 Measurements (Sensor 3):

Elapsed Time (min)	Bias V=0 C (pF)	Voltage Shift (V)	Est. Cfb (pF)	Cco (ppm)	Air Flow Rate (mL/min)	CO Flow Rate (mL/min)	Total Flow (mL/min)	Test Condition	Substrate Actual T (°C)
0	102.64	0.00							22.2
0	103.59	0.00	102.67	0.0	1000	0	1000	settle	22.2
10	103.66	0.15	102.67	25.3	1000	26	1026	exposure	22.5
20	103.90	0.00	102.67	0.0	1000	0	1000	settle	22.7
30	105.25	0.48	102.67	47.6	1000	50	1050	exposure	22.8
40	105.66	0.10	102.67	0.0	1000	0	1000	settle	22.8
50	104.95	0.30	102.67	90.9	1000	100	1100	exposure	23.0
60	105.21	0.15	102.67	0.0	1000	0	1000	settle	23.0
70	105.14	0.35	102.67	200.0	1000	250	1250	exposure	23.0
80	104.08	0.18	102.67	0.0	1000	0	1000	settle	23.2
90	105.50	0.38	102.67	411.8	1000	700	1700	exposure	23.2
100	105.00	0.20	102.67	0.0	1000	0	1000	settle	23.2
110	105.25	0.58	102.67	500.0	1000	1000	2000	exposure	23.3
120	105.17	0.23	102.67	0.0	1000	0	1000	settle	23.3
130	105.26	0.53	102.67	800.0	250	1000	1250	exposure	23.2
140	105.20	0.25	102.67	0.0	1000	0	1000	settle	23.3
150	104.98	0.49	102.67	1000.0	0	1000	1000	exposure	23.2

Test 3 Measurements (Al/Cu w/ 60 nm Pt Sensor):

Elapsed Time (min)	Bias V=0 C (pF)	Est. Cfb (pF)	Cco (ppm)	Air Flow Rate (mL/min)	CO Flow Rate (mL/min)	Total Flow (mL/min)	Test Condition	Substrate Actual T (°C)
0	141.72							22.2
0	140.94	143.00	0.0	1000	0	1000	settle	22.2
10	139.09	143.00	25.3	1000	26	1026	exposure	22.5
20	144.03	143.00	0.0	1000	0	1000	settle	22.7
30	145.05	143.00	47.6	1000	50	1050	exposure	22.8
40	144.16	143.00	0.0	1000	0	1000	settle	22.8
50	143.72	143.00	90.9	1000	100	1100	exposure	23.0
60	141.68	143.00	0.0	1000	0	1000	settle	23.0
70	144.69	143.00	200.0	1000	250	1250	exposure	23.0
80	145.17	143.00	0.0	1000	0	1000	settle	23.2
90	144.58	143.00	411.8	1000	700	1700	exposure	23.2
100	201.90	201.90	0.0	1000	0	1000	settle	23.2
110	202.40	201.90	500.0	1000	1000	2000	exposure	23.3
120	200.50	201.90	0.0	1000	0	1000	settle	23.3
130	200.50	201.90	800.0	250	1000	1250	exposure	23.2
140	200.50	201.90	0.0	1000	0	1000	settle	23.3
150	199.90	201.90	1000.0	0	1000	1000	exposure	23.2

Test 4 Measurements (Sensor 1):

Elapsed Time (min)	Bias V=0 C (pF)	? Est. Vfb (V)	Est. Cfb (pF)	Cco (ppm)	Air Flow Rate (mL/min)	CO Flow Rate (mL/min)	Total Flow (mL/min)	Test Condition	Substrate Actual T (°C)
0	99.62								23.0
10	99.65	0.00	99.65	0.0	1000	0	1000	settle	23.0
20	105.23	0.00	105.23	1000.0	0	1000	1000	exposure	23.1

Sensor 1 – Raw C-V Response Data for Gas Exposure Room Temperature Test

0 ppm			1000 ppm		
-35	9.90E-11	98.99	-35	1.05E-10	105.48
-34.22222	9.90E-11	98.98	-34.22222	1.05E-10	105.39
-33.44444	9.90E-11	98.96	-33.44444	1.05E-10	105.39
-32.66667	9.90E-11	98.98	-32.66667	1.05E-10	105.33
-31.88889	9.90E-11	99.00	-31.88889	1.05E-10	105.30
-31.11111	9.89E-11	98.94	-31.11111	1.05E-10	105.30
-30.33333	9.90E-11	98.97	-30.33333	1.05E-10	105.26
-29.55556	9.90E-11	98.99	-29.55556	1.05E-10	105.23
-28.77778	9.90E-11	98.99	-28.77778	1.05E-10	105.32
-28	9.90E-11	98.97	-28	1.05E-10	105.33
-27.22222	9.90E-11	98.99	-27.22222	1.05E-10	105.37
-26.44444	9.90E-11	98.98	-26.44444	1.05E-10	105.34
-25.66667	9.90E-11	98.98	-25.66667	1.05E-10	105.29
-24.88889	9.90E-11	98.98	-24.88889	1.05E-10	105.25
-24.11111	9.90E-11	98.99	-24.11111	1.05E-10	105.19
-23.33333	9.90E-11	98.99	-23.33333	1.05E-10	105.17
-22.55556	9.90E-11	98.98	-22.55556	1.05E-10	105.12
-21.77778	9.90E-11	98.99	-21.77778	1.05E-10	105.22
-21	9.90E-11	98.99	-21	1.05E-10	105.25
-20.22222	9.90E-11	99.02	-20.22222	1.05E-10	105.33
-19.44444	9.90E-11	98.99	-19.44444	1.05E-10	105.39
-18.66667	9.90E-11	98.99	-18.66667	1.05E-10	105.48
-17.88889	9.90E-11	99.00	-17.88889	1.06E-10	105.50
-17.11111	9.90E-11	99.00	-17.11111	1.05E-10	105.47
-16.33333	9.90E-11	98.95	-16.33333	1.06E-10	105.51
-15.55556	9.90E-11	98.99	-15.55556	1.06E-10	105.56
-14.77778	9.90E-11	99.00	-14.77778	1.06E-10	105.54
-14	9.90E-11	98.97	-14	1.06E-10	105.53
-13.22222	9.90E-11	98.98	-13.22222	1.06E-10	105.54
-12.44444	9.90E-11	98.99	-12.44444	1.06E-10	105.54
-11.66667	9.90E-11	98.99	-11.66667	1.06E-10	105.54
-10.88889	9.90E-11	98.99	-10.88889	1.06E-10	105.58
-10.11111	9.90E-11	99.00	-10.11111	1.06E-10	105.53
-9.333333	9.90E-11	99.00	-9.333333	1.06E-10	105.55
-8.555556	9.90E-11	98.96	-8.555556	1.06E-10	105.50
-7.777778	9.90E-11	98.95	-7.777778	1.06E-10	105.52
-7	9.90E-11	99.00	-7	1.06E-10	105.54
-6.222222	9.90E-11	98.99	-6.222222	1.06E-10	105.57
-5.444444	9.90E-11	98.99	-5.444444	1.06E-10	105.53
-4.666667	9.90E-11	98.99	-4.666667	1.06E-10	105.56
-3.888889	9.90E-11	98.97	-3.888889	1.06E-10	105.61
-3.111111	9.90E-11	98.96	-3.111111	1.06E-10	105.52
-2.333333	9.90E-11	98.96	-2.333333	1.06E-10	105.54
-1.555556	9.90E-11	98.96	-1.555556	1.06E-10	105.50
-0.777778	9.89E-11	98.92	-0.777778	1.06E-10	105.54
0	9.90E-11	98.95	0	1.06E-10	105.51
0.777778	9.90E-11	99.00	0.777778	1.06E-10	105.50
1.555556	9.89E-11	98.91	1.555556	1.06E-10	105.52
2.333333	9.90E-11	98.96	2.333333	1.06E-10	105.58
3.111111	9.89E-11	98.91	3.111111	1.06E-10	105.58
3.888889	9.89E-11	98.91	3.888889	1.06E-10	105.59
4.666667	9.89E-11	98.94	4.666667	1.06E-10	105.53
5.444444	9.89E-11	98.94	5.444444	1.06E-10	105.55
6.222222	9.90E-11	98.96	6.222222	1.06E-10	105.56
7	9.90E-11	98.98	7	1.06E-10	105.58
7.777778	9.89E-11	98.92	7.777778	1.06E-10	105.56
8.555556	9.90E-11	98.99	8.555556	1.06E-10	105.55
9.333333	9.90E-11	98.99	9.333333	1.06E-10	105.57
10.11111	9.90E-11	98.98	10.11111	1.06E-10	105.52
10.88889	9.90E-11	98.98	10.88889	1.06E-10	105.59
11.66667	9.90E-11	98.99	11.66667	1.06E-10	105.59
12.44444	9.90E-11	98.99	12.44444	1.06E-10	105.56
13.22222	9.90E-11	98.99	13.22222	1.06E-10	105.60
14	9.90E-11	98.98	14	1.06E-10	105.56
14.77778	9.90E-11	98.99	14.77778	1.06E-10	105.56
15.55556	9.90E-11	98.96	15.55556	1.06E-10	105.56
16.33333	9.90E-11	98.98	16.33333	1.06E-10	105.62
17.11111	9.90E-11	98.99	17.11111	1.06E-10	105.61
17.88889	9.90E-11	98.99	17.88889	1.06E-10	105.54
18.66667	9.90E-11	98.98	18.66667	1.06E-10	105.56
19.44444	9.90E-11	98.98	19.44444	1.06E-10	105.58
20.22222	9.90E-11	98.98	20.22222	1.06E-10	105.55

Sensor 2 – Raw C-V Response Data for Room Temperature Gas Exposure Test

0 ppm		25 ppm		50 ppm		100 ppm		200 ppm		400 ppm		500 pm		800 ppm		1000 ppm	
-10	67.20	-10	77.65	-10	80.82	-10	72.20	-10	72.87	-10	73.51	-10	72.84	-10	73.57	-10	73.83
-9.666667	67.00	-9.666667	65.60	-9.666667	74.30	-9.666667	72.70	-9.666667	74.93	-9.666667	73.57	-9.666667	74.87	-9.666667	75.60	-9.666667	75.85
-9.333333	69.00	-9.333333	66.80	-9.333333	75.00	-9.333333	74.30	-9.333333	76.33	-9.333333	75.56	-9.333333	76.33	-9.333333	77.05	-9.333333	77.27
-9	70.60	-9	68.40	-9	76.40	-9	75.90	-9	77.70	-9	77.04	-9	77.86	-9	78.33	-9	78.55
-8.666667	72.00	-8.666667	70.00	-8.666667	77.90	-8.666667	77.30	-8.666667	79.00	-8.666667	79.66	-8.666667	79.31	-8.666667	79.67	-8.666667	79.87
-8.333333	73.40	-8.333333	71.50	-8.333333	79.40	-8.333333	78.60	-8.333333	80.39	-8.333333	80.90	-8.333333	80.64	-8.333333	80.95	-8.333333	81.16
-8	74.70	-8	73.00	-8	80.80	-8	79.90	-8	81.60	-8	82.09	-8	81.75	-8	82.15	-8	82.51
-7.666667	76.00	-7.666667	74.50	-7.666667	82.00	-7.666667	81.30	-7.666667	82.80	-7.666667	83.31	-7.666667	83.04	-7.666667	83.43	-7.666667	83.65
-7.333333	77.30	-7.333333	75.80	-7.333333	83.40	-7.333333	82.50	-7.333333	84.00	-7.333333	84.57	-7.333333	84.31	-7.333333	84.66	-7.333333	84.91
-7	78.50	-7	77.20	-7	84.70	-7	83.80	-7	85.17	-7	85.68	-7	85.36	-7	85.83	-7	85.99
-6.666667	79.80	-6.666667	78.60	-6.666667	86.00	-6.666667	85.00	-6.666667	86.32	-6.666667	86.76	-6.666667	86.51	-6.666667	86.93	-6.666667	87.12
-6.333333	80.90	-6.333333	79.90	-6.333333	87.00	-6.333333	86.20	-6.333333	87.44	-6.333333	87.90	-6.333333	87.65	-6.333333	88.11	-6.333333	88.26
-6	82.20	-6	81.20	-6	88.40	-6	87.30	-6	88.55	-6	88.94	-6	88.76	-6	89.17	-6	89.28
-5.666667	83.40	-5.666667	82.50	-5.666667	89.40	-5.666667	88.50	-5.666667	89.48	-5.666667	89.92	-5.666667	89.71	-5.666667	90.27	-5.666667	90.34
-5.333333	84.50	-5.333333	83.80	-5.333333	90.50	-5.333333	89.70	-5.333333	90.61	-5.333333	90.11	-5.333333	90.82	-5.333333	91.42	-5.333333	91.37
-5	85.70	-5	85.00	-5	91.70	-5	90.70	-5	91.58	-5	91.90	-5	91.78	-5	92.37	-5	92.34
-4.666667	86.70	-4.666667	87.70	-4.666667	94.20	-4.666667	93.20	-4.666667	92.43	-4.666667	92.89	-4.666667	92.74	-4.666667	93.26	-4.666667	93.22
-4.333333	89.20	-4.333333	89.00	-4.333333	95.20	-4.333333	94.20	-4.333333	93.40	-4.333333	93.79	-4.333333	93.60	-4.333333	94.28	-4.333333	94.24
-4	90.10	-4	90.00	-4	96.10	-4	95.20	-4	94.08	-4	94.53	-4	94.39	-4	95.07	-4	94.91
-3.666667	90.90	-3.666667	91.00	-3.666667	96.90	-3.666667	95.80	-3.666667	94.76	-3.666667	95.15	-3.666667	95.02	-3.666667	95.70	-3.666667	95.60
-3.333333	91.40	-3.333333	91.80	-3.333333	97.60	-3.333333	96.30	-3.333333	95.13	-3.333333	95.52	-3.333333	95.42	-3.333333	96.25	-3.333333	96.01
-3	91.30	-3	92.30	-3	97.80	-3	96.50	-3	95.03	-3	95.41	-3	95.37	-3	96.12	-3	96.00
-2.666667	90.70	-2.666667	92.20	-2.666667	97.50	-2.666667	96.00	-2.666667	94.48	-2.666667	94.88	-2.666667	94.87	-2.666667	95.65	-2.666667	95.50
-2.333333	89.60	-2.333333	91.30	-2.333333	96.40	-2.333333	94.80	-2.333333	93.45	-2.333333	93.86	-2.333333	93.90	-2.333333	94.70	-2.333333	94.57
-2	88.20	-2	89.90	-2	94.80	-2	93.30	-2	92.07	-2	92.50	-2	92.49	-2	93.39	-2	93.28
-1.666667	86.70	-1.666667	88.20	-1.666667	92.80	-1.666667	91.60	-1.666667	90.26	-1.666667	91.01	-1.666667	91.10	-1.666667	91.94	-1.666667	91.80
-1.333333	84.90	-1.333333	86.20	-1.333333	90.60	-1.333333	89.80	-1.333333	88.82	-1.333333	89.37	-1.333333	89.41	-1.333333	90.34	-1.333333	90.18
-1	83.10	-1	84.30	-1	88.20	-1	87.80	-1	86.91	-1	87.53	-1	87.56	-1	88.49	-1	88.40
-0.666667	81.30	-0.666667	82.00	-0.666667	85.90	-0.666667	85.80	-0.666667	85.12	-0.666667	85.70	-0.666667	85.69	-0.666667	86.65	-0.666667	86.56
-0.333333	78.22	-0.333333	84.00	-0.333333	83.60	-0.333333	82.62	-0.333333	83.23	-0.333333	83.96	-0.333333	83.99	-0.333333	84.90	-0.333333	84.79
0	77.02	0	81.48	0	81.10	0	83.06	0	81.62	0	82.42	0	82.43	0	83.28	0	83.30
0.333333	76.32	0.333333	80.14	0.333333	79.72	0.333333	81.94	0.333333	80.06	0.333333	80.98	0.333333	80.93	0.333333	81.77	0.333333	81.90
0.666667	75.38	0.666667	78.92	0.666667	78.50	0.666667	80.18	0.666667	78.59	0.666667	79.52	0.666667	79.49	0.666667	80.31	0.666667	80.49
1	74.63	1	78.01	1	77.59	1	78.57	1	77.28	1	78.25	1	78.20	1	79.02	1	79.17
1.333333	73.87	1.333333	77.08	1.333333	76.68	1.333333	77.21	1.333333	76.39	1.333333	77.21	1.333333	77.15	1.333333	77.77	1.333333	78.06
1.666667	73.06	1.666667	76.08	1.666667	75.77	1.666667	76.01	1.666667	75.32	1.666667	76.26	1.666667	76.20	1.666667	76.76	1.666667	77.08
2	72.28	2	75.23	2	75.04	2	75.12	2	74.66	2	75.53	2	75.38	2	75.98	2	76.30
2.333333	71.60	2.333333	74.10	2.333333	74.46	2.333333	74.51	2.333333	73.97	2.333333	74.92	2.333333	74.83	2.333333	75.29	2.333333	75.56
2.666667	71.26	2.666667	74.22	2.666667	74.00	2.666667	73.68	2.666667	73.59	2.666667	74.40	2.666667	74.30	2.666667	74.67	2.666667	75.00
3	70.55	3	73.30	3	73.34	3	73.14	3	73.20	3	73.93	3	73.81	3	74.20	3	74.45
3.333333	69.84	3.333333	73.12	3.333333	73.25	3.333333	72.69	3.333333	73.02	3.333333	73.71	3.333333	73.43	3.333333	73.72	3.333333	74.00
3.666667	69.90	3.666667	73.42	3.666667	73.81	3.666667	72.14	3.666667	72.77	3.666667	73.26	3.666667	73.11	3.666667	73.37	3.666667	73.55
4	69.49	4	72.49	4	72.72	4	71.84	4	71.44	4	72.72	4	72.77	4	73.07	4	73.17
4.333333	69.32	4.333333	72.26	4.333333	72.49	4.333333	71.50	4.333333	72.05	4.333333	72.73	4.333333	72.51	4.333333	72.78	4.333333	72.89
4.666667	69.16	4.666667	70.72	4.666667	72.54	4.666667	71.39	4.666667	71.96	4.666667	72.37	4.666667	72.25	4.666667	72.48	4.666667	72.56
5	68.94	5	71.67	5	71.52	5	70.97	5	71.85	5	72.21	5	72.05	5	72.24	5	72.23
5.333333	68.54	5.333333	72.79	5.333333	71.87	5.333333	70.58	5.333333	71.66	5.333333	71.69	5.333333	71.81	5.333333	71.98	5.333333	72.00
5.666667	68.47	5.666667	71.21	5.666667	71.32	5.666667	70.60	5.666667	71.34	5.666667	71.83	5.666667	71.60	5.666667	71.85	5.666667	71.66
6	68.09	6	70.85	6	70.83	6	70.10	6	71.23	6	71.54	6	71.38	6	71.53	6	71.46
6.333333	68.06	6.333333	70.45	6.333333	70.05	6.333333	69.78	6.333333	70.86	6.333333	71.36	6.333333	71.10	6.333333	71.30	6.333333	71.20
6.666667	67.66	6.666667	59.31	6.666667	71.62	6.666667	69.55	6.666667	70.85	6.666667	71.09	6.666667	70.85	6.666667	71.00	6.666667	70.97
7	67.73	7	69.46	7	70.00	7	69.23	7	70.71	7	70.89	7	70.76	7	70.83	7	70.22
7.333333	67.52	7.333333	69.53	7.333333	69.06	7.333333	68.97	7.333333	70.33	7.333333	70.72	7.333333	69.70	7.333333	70.54	7.333333	69.98
7.666667	67.04	7.666667	66.91	7.666667	69.11	7.666667	67.99	7.666667	70.09	7.666667	68.17	7.666667	69.43	7.666667	70.26	7.666667	69.95
8	66.89	8	68.87	8	68.87	8	68.20	8	69.16	8	69.24	8	68.94	8	69.95	8	69.59
8.333333	66.82	8.333333	69.80	8.333333	70.02	8.333333	68.38	8.333333	68.77	8.333333	69.55	8.333333	69.00	8.333333	69.86	8.333333	69.67
8.666667	64.06	8.666667	68.92	8.666667	69.01	8.666667	67.95	8.666667	68.78	8.666667	68.83	8.666667	68.85	8.666667	69.57	8.666667	69.40
9	66.06	9	69.85	9	67.19	9	67.89	9	68.80	9	68.58	9	68.61	9	69.39	9	69.21
9.333333	65.71	9.333333	64.49	9.333333	68.12	9.333333	67.44	9.333333	68.58	9.333333	68.58	9.333333	68.31	9.333333	68.43	9.333333	69.42
9.666667	67.01	9.666667	67.44	9.666667	67.81	9.666667	67.19	9.666667	68.57	9.666667	68.52	9.666667	68.10	9.666667	68.36	9.666667	69.16
10	67.06	10	67.98	10	67.40	10	66.98	10	68.18	10	68.33	10	67.35	10	68.20	10	69.19

Sensor 2 – Raw C-V Response Data for R.T. Gas Exposure Test with +/- 5V Sweep

0 ppm		25 ppm		50 ppm		100 ppm		200 ppm		400 ppm		500 pm		800 ppm		1000 ppm	
-5	89.71	-5	89.73	-5	91.86	-5	92.78	-5	92.99	-5	93.45	-5	93.77	-5	93.89	-5	93.61
-4.666667	90.02	-4.666667	90.14	-4.666667	92.35	-4.666667	93.20	-4.666667	92.34	-4.666667	93.98	-4.666667	93.65	-4.666667	94.55	-4.666667	94.21
-4.333333	90.05	-4.333333	90.24	-4.333333	93.66	-4.333333	94.20	-4.333333	93.89	-4.333333	93.79	-4.333333	93.60	-4.333333	94.28	-4.333333	94.24
-4	90.10	-4	90.67	-4	93.70	-4	94.69	-4	94.97	-4	94.53	-4	94.39	-4	94.55	-4	94.91
-3.666667	90.90	-3.666667	90.77	-3.666667	93.51	-3.666667	94.57	-3.666667	95.05	-3.666667	95.15	-3.666667	95.02	-3.666667	95.70	-3.666667	95.60
-3.333333	91.40	-3.333333	91.04	-3.333333	93.55	-3.333333	95.10	-3.333333	95.13	-3.333333	95.52	-3.333333	95.42	-3.333333	95.71	-3.333333	96.01
-3	91.30	-3	91.66	-3	92.76	-3	94.97	-3	95.03	-3	95.41	-3	95.37	-3	95.62	-3	96.00
-2.666667	90.70	-2.666667	90.88	-2.666667	92.60	-2.666667	94.88	-2.666667	94.48	-2.666667	94.88	-2.666667	94.87	-2.666667	94.89	-2.666667	95.50
-2.333333	89.60	-2.333333	90.77	-2.333333	92.34	-2.333333	94.80	-2.333333	93.45	-2.333333	93.86	-2.333333	93.90	-2.333333	94.70	-2.333333	94.57
-2	88.20	-2	89.90	-2	91.56	-2	93.30	-2	92.07	-2	92.50	-2	92.49	-2	93.39	-2	93.28
-1.666667	86.70	-1.666667	88.20	-1.666667	90.45	-1.666667	91.60	-1.666667	90.26	-1.666667	91.01	-1.666667	91.10	-1.666667	91.94	-1.666667	91.80
-1.333333	84.90	-1.333333	86.20	-1.333333	88.87	-1.333333	89.80	-1.333333	88.82	-1.333333	89.37	-1.333333	89.41	-1.333333	90.34	-1.333333	90.18
-1	83.10	-1	84.30	-1	86.21	-1	87.80	-1	86.91	-1	87.53	-1	87.56	-1	88.49	-1	88.40
-0.666667	81.30	-0.666667	82.00	-0.666667	84.30	-0.666667	85.80	-0.666667	85.12	-0.666667	85.70	-0.666667	85.69	-0.666667	86.65	-0.666667	86.56
-0.333333	78.22	-0.333333	81.78	-0.333333	81.98	-0.333333	82.62	-0.333333	83.23	-0.333333	83.96	-0.333333	83.99	-0.333333	84.90	-0.333333	84.79
0	77.02	0	81.48	0	82.62	0	82.86	0	81.95	0	82.42	0	82.43	0	83.28	0	83.30
0.333333	76.32	0.333333	80.14	0.333333	79.72	0.333333	81.94	0.333333	80.06	0.333333	80.98	0.333333	80.93	0.333333	81.77	0.333333	81.90
0.666667	75.38	0.666667	78.92	0.666667	78.50	0.666667	80.18	0.666667	78.59	0.666667	79.52	0.666667	79.49	0.666667	80.31	0.666667	80.49
1	74.63	1	78.01	1	77.59	1	78.57	1	77.28	1	78.25	1	78.20	1	79.02	1	79.17
1.333333	73.87	1.333333	77.08	1.333333	76.68	1.333333	77.21	1.333333	76.39	1.333333	77.21	1.333333	77.15	1.333333	77.77	1.333333	78.06
1.666667	73.06	1.666667	76.08	1.666667	75.77	1.666667	76.01	1.666667	75.32	1.666667	76.26	1.666667	76.20	1.666667	76.76	1.666667	77.08
2	72.28	2	75.23	2	75.04	2	75.12	2	74.66	2	75.53	2	75.38	2	75.98	2	76.30
2.333333	71.60	2.333333	74.10	2.333333	74.46	2.333333	74.51	2.333333	73.97	2.333333	74.92	2.333333	74.83	2.333333	75.29	2.333333	75.56
2.666667	71.26	2.666667	74.22	2.666667	74.00	2.666667	73.68	2.666667	73.59	2.666667	74.40	2.666667	74.30	2.666667	74.67	2.666667	75.00
3	70.55	3	73.30	3	73.34	3	73.14	3	73.20	3	73.93	3	73.81	3	74.20	3	74.45
3.333333	69.84	3.333333	73.12	3.333333	73.25	3.333333	72.69	3.333333	73.02	3.333333	73.71	3.333333	73.43	3.333333	73.72	3.333333	74.00
3.666667	69.90	3.666667	73.42	3.666667	73.81	3.666667	72.14	3.666667	72.77	3.666667	73.26	3.666667	73.11	3.666667	73.37	3.666667	73.55
4	69.49	4	72.49	4	72.72	4	71.84	4	71.44	4	72.72	4	72.77	4	73.07	4	73.17
4.333333	69.32	4.333333	72.26	4.333333	72.49	4.333333	71.50	4.333333	72.05	4.333333	72.73	4.333333	72.51	4.333333	72.78	4.333333	72.89
4.666667	69.16	4.666667	70.72	4.666667	72.54	4.666667	71.39	4.666667	71.96	4.666667	72.37	4.666667	72.25	4.666667	72.48	4.666667	72.56
5	68.94	5	71.67	5	71.52	5	70.97	5	71.85	5	72.21	5	72.05	5	72.24	5	72.23

Sensor 3 – Raw C-V Response Data for Room Temperature Gas Exposure Test

0 ppm		25 ppm		50 ppm		100 ppm		200 ppm		400 ppm		500 pm		800 ppm		1000 ppm	
-10	103.77	-10	104.23	-10	105.78	-10	105.38	-10	105.75	-10	106.04	-10	105.72	-10	105.57	-10	105.49
-9.666667	90.51	-9.666667	89.10	-9.666667	92.20	-9.666667	84.50	-9.666667	84.50	-9.666667	86.00	-9.666667	89.00	-9.666667	88.43	-9.666667	88.70
-9.333333	90.89	-9.333333	89.60	-9.333333	92.90	-9.333333	85.70	-9.333333	85.70	-9.333333	86.50	-9.333333	89.30	-9.333333	89.08	-9.333333	89.50
-9	92.04	-9	90.80	-9	94.10	-9	87.00	-9	87.20	-9	88.00	-9	90.50	-9	90.27	-9	90.70
-8.666667	93.35	-8.666667	92.20	-8.666667	95.30	-8.666667	88.60	-8.666667	88.70	-8.666667	89.50	-8.666667	91.90	-8.666667	91.62	-8.666667	92.10
-8.333333	94.54	-8.333333	93.60	-8.333333	96.50	-8.333333	90.20	-8.333333	90.20	-8.333333	90.90	-8.333333	93.40	-8.333333	92.84	-8.333333	93.40
-8	95.67	-8	94.60	-8	97.60	-8	91.50	-8	91.70	-8	92.40	-8	94.70	-8	94.21	-8	94.70
-7.666667	96.95	-7.666667	95.80	-7.666667	98.70	-7.666667	93.20	-7.666667	93.10	-7.666667	93.80	-7.666667	95.90	-7.666667	95.74	-7.666667	96.00
-7.333333	97.97	-7.333333	96.90	-7.333333	99.80	-7.333333	94.70	-7.333333	94.50	-7.333333	95.10	-7.333333	97.20	-7.333333	96.71	-7.333333	97.10
-7	99.13	-7	98.10	-7	100.80	-7	96.00	-7	95.80	-7	96.50	-7	98.40	-7	98.08	-7	98.30
-6.666667	100.15	-6.666667	99.20	-6.666667	102.00	-6.666667	97.20	-6.666667	97.10	-6.666667	97.80	-6.666667	99.60	-6.666667	99.29	-6.666667	99.60
-6.333333	101.01	-6.333333	100.30	-6.333333	102.90	-6.333333	98.60	-6.333333	98.60	-6.333333	99.20	-6.333333	100.70	-6.333333	100.32	-6.333333	100.60
-6	102.08	-6	101.40	-6	103.90	-6	99.90	-6	99.90	-6	100.40	-6	102.00	-6	101.57	-6	101.80
-5.666667	103.04	-5.666667	102.50	-5.666667	104.90	-5.666667	101.30	-5.666667	101.20	-5.666667	101.70	-5.666667	103.20	-5.666667	102.75	-5.666667	103.00
-5.333333	104.04	-5.333333	103.50	-5.333333	105.80	-5.333333	102.50	-5.333333	102.50	-5.333333	103.00	-5.333333	104.10	-5.333333	103.88	-5.333333	104.10
-5	105.00	-5	106.10	-5	108.30	-5	105.30	-5	105.30	-5	105.80	-5	106.80	-5	105.03	-5	106.60
-4.666667	105.95	-4.666667	107.10	-4.666667	109.20	-4.666667	106.50	-4.666667	106.60	-4.666667	107.00	-4.666667	108.00	-4.666667	106.20	-4.666667	107.70
-4.333333	106.93	-4.333333	108.20	-4.333333	110.30	-4.333333	107.90	-4.333333	107.90	-4.333333	108.40	-4.333333	109.10	-4.333333	107.35	-4.333333	108.90
-4	108.01	-4	109.20	-4	111.30	-4	109.10	-4	109.10	-4	109.50	-4	110.20	-4	108.44	-4	110.10
-3.666667	109.00	-3.666667	110.20	-3.666667	112.20	-3.666667	110.20	-3.666667	110.40	-3.666667	110.80	-3.666667	111.30	-3.666667	109.55	-3.666667	111.20
-3.333333	109.78	-3.333333	111.30	-3.333333	113.20	-3.333333	111.50	-3.333333	111.60	-3.333333	111.90	-3.333333	112.40	-3.333333	110.52	-3.333333	112.30
-3	110.62	-3	112.20	-3	114.10	-3	112.60	-3	112.70	-3	113.10	-3	113.30	-3	111.59	-3	113.10
-2.666667	111.35	-2.666667	112.90	-2.666667	114.70	-2.666667	113.40	-2.666667	113.50	-2.666667	113.90	-2.666667	114.10	-2.666667	112.26	-2.666667	113.80
-2.333333	111.47	-2.333333	113.00	-2.333333	114.80	-2.333333	113.80	-2.333333	113.90	-2.333333	114.20	-2.333333	114.30	-2.333333	112.62	-2.333333	114.20
-2	111.08	-2	112.60	-2	114.30	-2	113.40	-2	113.60	-2	113.80	-2	113.90	-2	112.32	-2	113.60
-1.666667	109.99	-1.666667	111.40	-1.666667	113.00	-1.666667	112.40	-1.666667	112.50	-1.666667	112.80	-1.666667	112.70	-1.666667	111.36	-1.666667	112.50
-1.333333	108.60	-1.333333	109.90	-1.333333	111.60	-1.333333	111.00	-1.333333	111.10	-1.333333	111.50	-1.333333	111.30	-1.333333	110.05	-1.333333	111.10
-1	107.24	-1	108.50	-1	110.10	-1	109.60	-1	109.80	-1	110.10	-1	110.00	-1	108.81	-1	109.60
-0.666667	105.82	-0.666667	105.46	-0.666667	107.07	-0.666667	106.64	-0.666667	106.81	-0.666667	107.10	-0.666667	108.40	-0.666667	107.48	-0.666667	108.10
-0.333333	104.51	-0.333333	103.98	-0.333333	105.61	-0.333333	105.21	-0.333333	105.39	-0.333333	105.69	-0.333333	106.30	-0.333333	106.23	-0.333333	106.03
0	103.59	0	103.66	0	105.25	0	104.95	0	105.14	0	105.50	0	105.25	0	105.26	0	104.98
0.333333	103.02	0.333333	103.24	0.333333	104.82	0.333333	104.55	0.333333	104.74	0.333333	105.05	0.333333	104.74	0.333333	104.68	0.333333	104.46
0.666667	102.74	0.666667	102.96	0.666667	104.52	0.666667	104.28	0.666667	104.48	0.666667	104.79	0.666667	104.42	0.666667	104.45	0.666667	104.16
1	102.67	1	102.97	1	104.50	1	104.28	1	104.48	1	104.78	1	104.42	1	104.44	1	104.15
1.333333	102.52	1.333333	102.79	1.333333	104.34	1.333333	104.11	1.333333	104.32	1.333333	104.60	1.333333	104.25	1.333333	104.27	1.333333	103.99
1.666667	102.34	1.666667	102.57	1.666667	104.10	1.666667	103.88	1.666667	104.09	1.666667	104.27	1.666667	104.03	1.666667	104.03	1.666667	103.76
2	102.02	2	102.34	2	103.89	2	103.66	2	103.86	2	104.14	2	103.81	2	103.80	2	103.54
2.333333	101.85	2.333333	102.14	2.333333	103.68	2.333333	103.46	2.333333	103.65	2.333333	103.93	2.333333	103.60	2.333333	103.58	2.333333	103.34
2.666667	101.65	2.666667	101.94	2.666667	103.49	2.666667	103.25	2.666667	103.45	2.666667	103.73	2.666667	103.41	2.666667	103.38	2.666667	103.14
3	101.45	3	101.74	3	103.27	3	103.02	3	103.22	3	103.49	3	103.17	3	103.12	3	102.90
3.333333	101.21	3.333333	101.47	3.333333	102.99	3.333333	102.74	3.333333	102.90	3.333333	103.13	3.333333	102.85	3.333333	102.79	3.333333	102.58
3.666667	100.82	3.666667	101.03	3.666667	102.55	3.666667	102.28	3.666667	102.39	3.666667	102.59	3.666667	102.33	3.666667	102.28	3.666667	102.05
4	100.30	4	100.41	4	101.91	4	101.62	4	101.68	4	101.78	4	101.60	4	101.50	4	101.29
4.333333	99.54	4.333333	99.60	4.333333	101.07	4.333333	100.75	4.333333	100.74	4.333333	100.77	4.333333	100.66	4.333333	100.49	4.333333	100.31
4.666667	98.56	4.666667	98.58	4.666667	100.01	4.666667	99.66	4.666667	99.58	4.666667	99.72	4.666667	99.49	4.666667	99.32	4.666667	99.08
5	97.33	5	97.33	5	98.74	5	98.33	5	98.23	5	98.39	5	98.11	5	97.89	5	97.68
5.333333	95.94	5.333333	95.89	5.333333	97.26	5.333333	96.80	5.333333	96.65	5.333333	96.83	5.333333	96.52	5.333333	96.29	5.333333	96.05
5.666667	94.42	5.666667	94.28	5.666667	95.57	5.666667	95.04	5.666667	94.88	5.666667	95.09	5.666667	94.77	5.666667	94.49	5.666667	94.22
6	92.72	6	92.52	6	93.73	6	93.14	6	92.98	6	93.15	6	92.86	6	92.52	6	92.27
6.333333	90.89	6.333333	90.62	6.333333	91.77	6.333333	91.12	6.333333	90.95	6.333333	91.12	6.333333	90.86	6.333333	90.47	6.333333	90.23
6.666667	88.97	6.666667	88.62	6.666667	89.72	6.666667	88.99	6.666667	88.84	6.666667	89.01	6.666667	88.76	6.666667	88.33	6.666667	88.06
7	86.70	7	86.53	7	87.28	7	86.82	7	86.62	7	86.78	7	86.54	7	86.05	7	85.84
7.333333	84.67	7.333333	84.40	7.333333	85.20	7.333333	84.52	7.333333	84.37	7.333333	84.50	7.333333	84.28	7.333333	83.89	7.333333	83.55
7.666667	82.29	7.666667	81.85	7.666667	82.95	7.666667	82.19	7.666667	82.05	7.666667	81.88	7.666667	81.69	7.666667	81.31	7.666667	81.00
8	80.10	8	79.62	8	80.34	8	79.79	8	79.61	8	79.63	8	79.44	8	79.05	8	78.72
8.333333	77.89	8.333333	77.01	8.333333	78.03	8.333333	77.09	8.333333	76.89	8.333333	76.94	8.333333	76.80	8.333333	76.48	8.333333	76.08
8.666667	75.22	8.666667	74.72	8.666667	75.35	8.666667	74.70	8.666667	74.55	8.666667	74.57	8.666667	74.48	8.666667	74.12	8.666667	73.73
9	72.77	9	71.95	9	72.96	9	71.92	9	71.78	9	71.84	9	71.73	9	71.36	9	71.00
9.333333	70.02	9.333333	69.59	9.333333	70.24	9.333333	69.52	9.333333	69.36	9.333333	69.39	9.333333	69.39	9.333333	69.01	9.333333	68.70
9.666667	67.51	9.666667	66.78	9.666667	67.83	9.666667	66.69	9.666667	66.54	9.666667	66.58	9.666667	66.67	9.666667	66.38	9.666667	65.92
10	64.85	10	64.32	10	65.00	10	64.20	10	64.00	10	64.12	10	64.25	10	63.91	10	63.49

Al/Cu CV Disk Sensor – Raw C-V Response Data for Room Temperature Gas Exposure Test

0 ppm		50 ppm		100 ppm		200 ppm		400 ppm		500 pm		800 ppm		1000 ppm	
-10	141.79	-10	145.89	-10	143.77	-10	144.74	-10	144.58	-10	203.10	-10	201.50	-10	200.50
-9.666667	128.50	-9.666667	145.51	-9.666667	130.40	-9.666667	131.70	-9.666667	131.70	-9.666667	306.70	-9.666667	295.30	-9.666667	293.40
-9.333333	128.60	-9.333333	133.00	-9.333333	130.50	-9.333333	131.70	-9.333333	131.90	-9.333333	290.00	-9.333333	285.30	-9.333333	285.80
-9	128.80	-9	133.00	-9	130.80	-9	131.90	-9	132.20	-9	287.60	-9	282.90	-9	280.90
-8.666667	129.10	-8.666667	133.40	-8.666667	131.10	-8.666667	132.30	-8.666667	132.60	-8.666667	285.70	-8.666667	280.20	-8.666667	278.30
-8.333333	129.40	-8.333333	133.70	-8.333333	131.50	-8.333333	132.80	-8.333333	132.90	-8.333333	283.60	-8.333333	277.60	-8.333333	275.90
-8	129.70	-8	134.10	-8	132.00	-8	133.10	-8	133.30	-8	281.50	-8	275.00	-8	273.30
-7.666667	130.10	-7.666667	134.50	-7.666667	132.30	-7.666667	133.60	-7.666667	133.70	-7.666667	279.40	-7.666667	272.70	-7.666667	270.90
-7.333333	130.60	-7.333333	135.00	-7.333333	132.80	-7.333333	134.10	-7.333333	134.20	-7.333333	277.20	-7.333333	269.90	-7.333333	268.40
-7	131.10	-7	135.50	-7	133.50	-7	134.60	-7	134.70	-7	275.10	-7	267.50	-7	265.90
-6.666667	131.90	-6.666667	136.00	-6.666667	134.00	-6.666667	135.20	-6.666667	135.30	-6.666667	273.00	-6.666667	265.00	-6.666667	263.30
-6.333333	132.70	-6.333333	136.70	-6.333333	134.80	-6.333333	135.90	-6.333333	135.90	-6.333333	270.60	-6.333333	262.40	-6.333333	260.80
-6	133.50	-6	137.67	-6	135.40	-6	136.60	-6	136.70	-6	268.20	-6	259.90	-6	258.40
-5.666667	135.07	-5.666667	137.91	-5.666667	136.20	-5.666667	137.40	-5.666667	137.30	-5.666667	265.50	-5.666667	257.20	-5.666667	255.70
-5.333333	135.41	-5.333333	138.67	-5.333333	136.90	-5.333333	138.00	-5.333333	138.00	-5.333333	262.60	-5.333333	254.50	-5.333333	253.10
-5	136.41	-5	139.43	-5	137.99	-5	139.06	-5	138.70	-5	259.70	-5	251.90	-5	250.40
-4.666667	137.53	-4.666667	140.12	-4.666667	138.11	-4.666667	139.21	-4.666667	139.20	-4.666667	256.60	-4.666667	249.00	-4.666667	247.60
-4.333333	138.53	-4.333333	140.80	-4.333333	138.74	-4.333333	139.80	-4.333333	140.22	-4.333333	253.40	-4.333333	246.10	-4.333333	244.70
-4	139.47	-4	141.41	-4	139.36	-4	140.38	-4	140.23	-4	250.00	-4	243.10	-4	241.70
-3.666667	140.21	-3.666667	141.94	-3.666667	139.90	-3.666667	140.92	-3.666667	140.76	-3.666667	246.50	-3.666667	240.20	-3.666667	238.70
-3.333333	140.76	-3.333333	142.49	-3.333333	140.41	-3.333333	141.43	-3.333333	141.33	-3.333333	243.00	-3.333333	237.00	-3.333333	235.50
-3	141.21	-3	142.98	-3	140.96	-3	141.98	-3	141.90	-3	239.30	-3	233.80	-3	232.50
-2.666667	141.51	-2.666667	143.50	-2.666667	141.55	-2.666667	142.56	-2.666667	142.48	-2.666667	235.70	-2.666667	230.60	-2.666667	229.30
-2.333333	141.72	-2.333333	144.02	-2.333333	142.11	-2.333333	143.17	-2.333333	143.12	-2.333333	231.70	-2.333333	227.10	-2.333333	225.90
-2	141.95	-2	144.68	-2	142.80	-2	143.82	-2	143.88	-2	227.60	-2	223.60	-2	222.50
-1.666667	142.13	-1.666667	145.29	-1.666667	143.40	-1.666667	144.44	-1.666667	145.20	-1.666667	223.50	-1.666667	220.00	-1.666667	218.90
-1.333333	142.40	-1.333333	146.50	-1.333333	144.70	-1.333333	145.70	-1.333333	145.70	-1.333333	219.40	-1.333333	216.20	-1.333333	215.20
-1	143.20	-1	146.70	-1	144.90	-1	145.90	-1	145.80	-1	215.60	-1	212.80	-1	211.90
-0.666667	143.00	-0.666667	146.80	-0.666667	144.90	-0.666667	145.90	-0.666667	145.80	-0.666667	211.50	-0.666667	209.10	-0.666667	208.30
-0.333333	141.35	-0.333333	145.13	-0.333333	145.20	-0.333333	146.20	-0.333333	146.20	-0.333333	206.70	-0.333333	204.70	-0.333333	204.00
0	140.94	0	145.05	0	143.72	0	144.69	0	144.58	0	202.40	0	200.50	0	199.90
0.333333	142.25	0.333333	146.88	0.333333	144.86	0.333333	145.85	0.333333	145.76	0.333333	199.30	0.333333	197.90	0.333333	197.30
0.666667	143.47	0.666667	148.46	0.666667	146.65	0.666667	147.62	0.666667	147.69	0.666667	198.00	0.666667	196.90	0.666667	196.20
1	144.50	1	149.92	1	148.17	1	149.15	1	149.28	1	197.10	1	196.20	1	195.60
1.333333	144.89	1.333333	150.87	1.333333	149.18	1.333333	150.19	1.333333	150.40	1.333333	195.00	1.333333	194.50	1.333333	193.90
1.666667	144.78	1.666667	150.95	1.666667	149.41	1.666667	150.38	1.666667	150.62	1.666667	192.40	1.666667	192.00	1.666667	191.60
2	144.65	2	150.90	2	149.31	2	150.39	2	150.61	2	190.00	2	190.00	2	189.50
2.333333	144.62	2.333333	150.91	2.333333	149.32	2.333333	150.38	2.333333	150.59	2.333333	188.20	2.333333	188.30	2.333333	187.90
2.666667	144.63	2.666667	150.97	2.666667	149.33	2.666667	150.47	2.666667	150.64	2.666667	186.50	2.666667	186.80	2.666667	186.40
3	144.67	3	150.98	3	149.41	3	150.56	3	150.67	3	185.00	3	185.50	3	185.10
3.333333	144.78	3.333333	151.05	3.333333	149.44	3.333333	150.64	3.333333	150.73	3.333333	183.70	3.333333	184.30	3.333333	183.80
3.666667	144.86	3.666667	151.17	3.666667	149.58	3.666667	150.76	3.666667	150.87	3.666667	182.50	3.666667	183.20	3.666667	182.80
4	144.99	4	151.22	4	149.63	4	150.88	4	150.95	4	181.30	4	182.30	4	181.90
4.333333	145.10	4.333333	151.34	4.333333	149.74	4.333333	151.04	4.333333	151.08	4.333333	180.20	4.333333	181.40	4.333333	180.90
4.666667	145.23	4.666667	151.47	4.666667	149.86	4.666667	151.18	4.666667	151.20	4.666667	179.40	4.666667	180.50	4.666667	180.00
5	145.33	5	151.57	5	149.98	5	151.28	5	151.33	5	178.60	5	179.80	5	179.30
5.333333	145.46	5.333333	151.64	5.333333	150.08	5.333333	151.40	5.333333	151.47	5.333333	177.80	5.333333	179.10	5.333333	178.60
5.666667	145.57	5.666667	151.75	5.666667	150.19	5.666667	151.45	5.666667	151.58	5.666667	176.90	5.666667	178.40	5.666667	177.80
6	145.67	6	151.84	6	150.28	6	151.54	6	151.68	6	176.10	6	177.60	6	177.20
6.333333	145.76	6.333333	151.92	6.333333	150.38	6.333333	151.64	6.333333	151.78	6.333333	175.40	6.333333	177.00	6.333333	176.50
6.666667	145.79	6.666667	151.97	6.666667	150.46	6.666667	151.75	6.666667	151.91	6.666667	174.60	6.666667	176.40	6.666667	175.80
7	145.86	7	152.01	7	150.50	7	151.82	7	151.99	7	174.00	7	175.70	7	175.20
7.333333	145.97	7.333333	152.07	7.333333	150.59	7.333333	152.16	7.333333	152.06	7.333333	173.20	7.333333	175.20	7.333333	174.60
7.666667	146.03	7.666667	152.12	7.666667	150.65	7.666667	152.26	7.666667	152.17	7.666667	172.60	7.666667	174.60	7.666667	173.90
8	146.06	8	152.19	8	150.71	8	152.31	8	152.23	8	171.90	8	173.90	8	173.40
8.333333	146.09	8.333333	152.21	8.333333	150.76	8.333333	152.53	8.333333	152.31	8.333333	171.20	8.333333	173.30	8.333333	172.60
8.666667	146.15	8.666667	152.22	8.666667	150.78	8.666667	152.63	8.666667	152.36	8.666667	170.50	8.666667	172.70	8.666667	172.00
9	146.14	9	152.27	9	150.84	9	152.65	9	152.44	9	169.80	9	172.10	9	171.30
9.333333	146.14	9.333333	152.28	9.333333	150.86	9.333333	152.69	9.333333	152.48	9.333333	169.10	9.333333	171.40	9.333333	170.70
9.666667	146.15	9.666667	152.27	9.666667	150.83	9.666667	152.71	9.666667	152.52	9.666667	168.40	9.666667	169.70	9.666667	170.10
10	146.19	10	152.29	10	150.67	10	152.72	10	152.56	10	167.70	10	169.10	10	169.30

Sensor C-V Response Observations for 200°C Gas Exposure Test

30nm Gate High Temperature Test
T = 200 C

Measurements: *Jeffrey C. Hunter, OGI, July 26, 2003*

Elapsed Time (min)	Bias V=0 C (pF)	Est. Cfb (pF)	Cco (ppm)	Air Flow Rate (mL/min)	CO Flow Rate (mL/min)	Total Flow (mL/min)	Test Condition	Substrate Actual T (°C)	Comments
0	89.80							74.8	
0	84.30	81.69						90.1	Initial measurement at 0V bias P-type response, not much depletion
10	122.41	151.20	0.0	1000	0	1000	settle	199.5	Start test.
20	123.01	123.01	1000.0	0	1000	1000	exposure	156.2	Finish test No capacitance peak >125pF Flat band appears to be around 0V. Gaussian looking with more depletion

AlCu Gate High Temperature Test
T = 200 C

Measurements: *Jeffrey C. Hunter, OGI, July 27, 2003*

Elapsed Time (min)	Bias V=0 C (pF)	Est. Cfb (pF)	Cco (ppm)	Air Flow Rate (mL/min)	CO Flow Rate (mL/min)	Total Flow (mL/min)	Test Condition	Substrate Actual T (°C)	Comments
0	89.80							74.8	
0	84.30	81.69						90.1	Initial measurement at 0V bias P-type response, not much depletion
10	-119.90	-118.40	0.0	1000	0	1000	settle	199.5	Start test. Get a Gaussian bell curve
20	-109.10	-118.40	1000.0	0	1000	1000	exposure	197.2	Finish test Same type of curve Variac set at 140V @ 67%

Measurements: *Jeffrey C. Hunter, OGI, July 27, 2003*

Elapsed Time (min)	Bias V=0 C (pF)	Est. Cfb (pF)	Cco (ppm)	Air Flow Rate (mL/min)	CO Flow Rate (mL/min)	Total Flow (mL/min)	Test Condition	Substrate Actual T (°C)	Comments
0									Initial measurement at 0V bias
10	122.41	122.41	0.0	1000	0	1000	settle	154.9	Start test. Rise by 25pF with heating substrate
20	118.52	118.52	1000.0	0	1000	1000	exposure	155.5	Finish test Variac set at 140V @ 67%

Biographical Sketch

Jeffrey C. Hunter is a senior engineer and group leader in Intel's Technology and Manufacturing Group. He joined Intel in 1991 and is currently responsible for the definition, development and deployment of advanced material handling and process flow automation systems. He has received numerous academic and professional awards and honors including the 2000 Intel Achievement Award for contributions to automated material handling enabling Intel's transition to 300mm wafer fabrication. He received his bachelor of science in electrical engineering from the University of New Mexico and master of science in electrical engineering from the Oregon Graduate Institute of Science and Engineering.